Journal of Controlled Release 377 (2025) 661–674

Contents lists available at ScienceDirect

Journal of Controlled Release

journal homepage: www.elsevier.com/locate/jconrel

Nanoparticulate drug combination inhibits DNA damage repair and PD-L1 expression in BRCA-mutant and wild type triple-negative breast cancer

Ibrahim Alradwan [a,c,1], Pei Zhi [a,1], Tian Zhang [a], HoYin Lip [a], Abdulmottaleb Zetrini [a], Chunsheng He [a], Jeffrey T. Henderson [a], Andrew M. Rauth [b], Xiao Yu Wu [a,*]

[a] Advanced Pharmaceutics and Drug Delivery Laboratory, Leslie Dan Faculty of Pharmacy, University of Toronto, 144 College Street, Toronto M5S 3M2, Ontario, Canada
[b] Departments of Medical Biophysics and Radiation Oncology, University of Toronto, 610 University Ave, Toronto M5G 2M9, Ontario, Canada
[c] Advanced Diagnostics and Therapeutics Institute, King Abdulaziz City for Science and Technology (KACST), Riyadh 11461, Saudi Arabia

ARTICLE INFO

Keywords:
Multitargeting nanoparticles
Drug combination
DNA damage repair
PD-L1 expression
BRCA mutation
Triple-negative breast cancer

ABSTRACT

The high mortality rate associated with metastatic breast cancer presents a significant global challenge. Inherent and chemotherapy-induced DNA damage repair, alongside immunosuppression, drastically contribute to triple-negative breast cancer (TNBC) relapse and metastasis. While poly (ADP-ribose) polymerase (PARP) inhibitors such as olaparib show effectiveness against BRCA1-mutant TNBC, they may lead to drug resistance and reduced efficacy due to increased programmed death-ligand 1 (PD-L1) expression. Our study explored the use of polymer-lipid nanoparticles (PLN) loaded with doxorubicin (DOX) and oligomeric hyaluronic acid (oHA), functionalized iRGD-peptide for integrins targeting (iRGD-DOX-oHA-PLN), to prevent TNBC immunosuppression, DNA repair, and metastasis. The results demonstrate that the iRGD-DOX-oHA-PLNs efficiently downregulated single and double-strand DNA repair proteins and enhanced DNA damage while decreasing PD-L1 expression compared to olaparib. Accordingly, iRGD-DOX-oHA-PLN treatment showed significantly higher efficiency in reducing levels of primary tumor growth and numbers of metastases to the lung and liver compared to olaparib *in vitro* and *in vivo* in both BRCA1-mutant and wild type TNBC orthotopic xenograft models.

1. Introduction

Among the various breast cancer subtypes, triple-negative breast cancer (TNBC) is distinguished by a markedly worse prognosis, reduced duration of progression-free survival, higher rate of metastatic recurrence, and high mortality rate [1,2]. TNBC, representing 15–20 % of all breast cancer diagnoses, is molecularly defined by its absence of estrogen receptor (ER), progesterone receptor (PR), and human epidermal growth factor receptor 2 (HER2) markers [3]. These features make TNBC carcinomas non-responsive to the available traditional hormonal and targeted breast cancer therapies [4]. Therefore, conventional chemotherapy after surgery is the standard of care for TNBC treatment. Despite the initial response to taxanes or the anthracycline doxorubicin (DOX), recurrence and metastases dramatically decrease the five-year overall survival rate to as low as ~11 % [5]. Patients with metastatic TNBC who are programmed death-ligand 1 (PD-L1)-positive are qualified to be treated with atezolizumab plus nab-paclitaxel combination [6].

Several interrelated challenges, including reduced drug accumulation and penetration, inadequate cellular uptake, and prolonged drug release timelines, often compromise the effectiveness of treatments to prevent metastasis [7–9]. These factors collectively lead to insufficient drug concentrations at the target metastatic locations [7]. Additionally, therapeutic strategies focused on a singular carcinogenic or metastatic pathway only deliver a subtherapeutic dose that may unintentionally accelerate the development of tumor resistance and further the metastatic spread [10]. In this milieu, the nanosized drug delivery systems designed for tumor-specific targeting and facilitation of controlled drug release emerge as pivotal innovations against drug resistance and chemotherapy failure due to the lack of definite targeting of cancer cells or their metastatic pathways, especially those involved in DNA repair or immunosuppression [9,11–13].

Mutations in the breast cancer susceptibility genes BRCA1 and BRCA2 are significantly more prevalent in patients diagnosed with

* Corresponding author.
E-mail address: sxy.wu@utoronto.ca (X.Y. Wu).
[1] Ibrahim Alradwan and Pei Zhi, it signifies equal contribution to the manuscript

https://doi.org/10.1016/j.jconrel.2024.11.061
Received 30 June 2024; Received in revised form 18 November 2024; Accepted 22 November 2024
Available online 30 November 2024

triple-negative breast cancer (TNBC) [14]. Specifically, ~ 70 % of individuals with TNBC exhibit BRCA1 mutations, while approximately ~23 % show mutations in BRCA2 [15]. The poly(ADP-ribose) polymerase (PARP) inhibitors have demonstrated efficacy in tumors exhibiting compromised DNA repair capabilities, notably those harboring BRCA1/2 mutations [16–18]. Nonetheless, despite the initial efficacy, resistance to PARP inhibitors has been observed in approximately 40 % of patients [19], possibly, due to reactivation of the homologous recombination (HR) double-strand break (DSB) DNA repair pathway through either BRCA1/2 reversion mutations or overexpression of RAD51 recombinase, as well as the increased activity of drug efflux pumps [20–22]. Administration of the PARP inhibitor olaparib has also been found to elevate the expression of the immune checkpoint protein, PD-L1, to foster an immunosuppressive tumor microenvironment and diminish drug effectiveness [23]. Recent approaches have proposed combining PARP inhibitors with immune checkpoint inhibitors (ICIs) or phosphoinositide-3-kinase (PI3K) inhibitors to combat the cancer resistance to PARP inhibitors [24,25]. Nonetheless, such ICIs have high costs, side effects, and drug resistance and might have limited efficacy in BRCA mutant and non-mutant TNBC [22,26–28].

The tumor microenvironment enriched with high molecular weight hyaluronic acid (HA), overexpression of the receptors-cluster of differentiation 44 (CD44) and receptor for hyaluronan-mediated motility (RHAMM), plays a crucial role in promoting metastasis in aggressive cancers such as TNBC, likely through the activation of PI3K/AKT and MAPK/ERK signaling pathways [29–32]. These metastasis pathways exhibit a well-characterized influence over tumor cell growth, cancer immunity, and DNA repair proteins expression [33]. As such, significant interest has also been generated in the potential for combinatorial therapy of PARP inhibitors with PI3K or MAPK inhibitors [33–36], as these pathways can regulate PD-L1 expression in cancer cells [37,38]. In addition, the HA polymer has been extensively studied as a targeting moiety for CD44 when included in nanoparticle (NP) formulations but rarely as a bioactive drug involved in cell signaling [39–41]. In contrast, the oligomer hyaluronic acid (oHA) has been shown to sensitize breast cancer to chemotherapy by reducing resistance proteins (BCRP) and P-glycoprotein (P-gp) [42–45]. In this regard, DOX has been shown to reduce PD-L1 expression levels in a TNBC cell model, likely mediated by

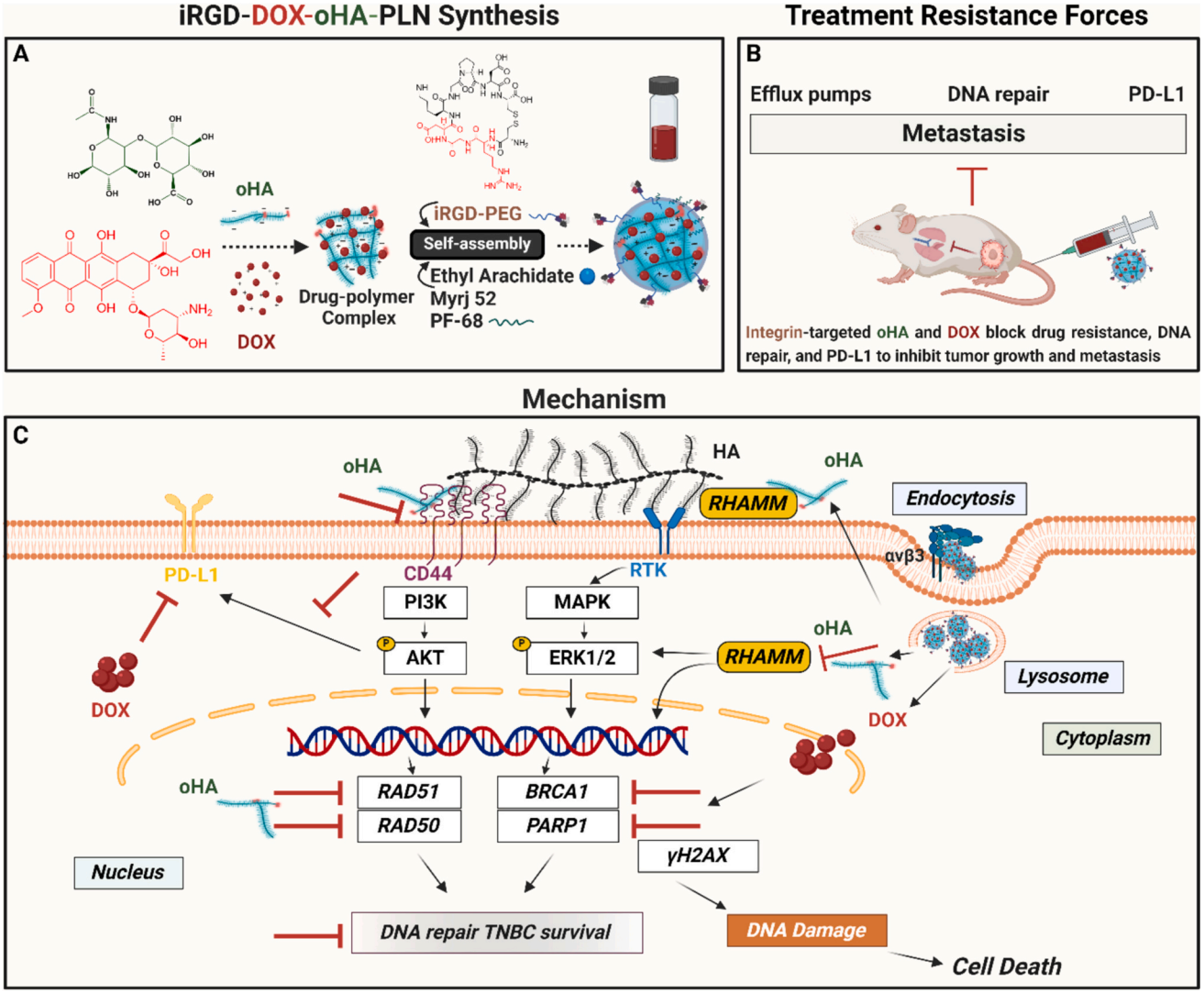

Fig. 1. Scheme of the combinational therapy proposed mechanism. (A) Self-assembly of iRGD-DOX-oHA-PLN by microemulsion technology. (B) A diagram of the intravenously (i.v.) injected formulation to work against the forces of treatment failure and tumor metastasis. (C) The proposed mechanism of iRGD-DOX-oHA-PLN outlines potential functions derived from the signal-regulating properties of oHA and the cytotoxicity of DOX. oHA inhibits CD44 and RHAMM signaling, thereby altering PI3K/AKT and MAPK/ERK pathways and impairing DNA damage repair by reducing critical repair proteins such as BRCA1, RAD50, RAD51, and PARP1. As a result, the efficacy of DOX in inducing DNA damage could be amplified, as evidenced by increased γH2AX levels. The PD-L1 expression level might be downregulated due to the combined effects of both DOX and oHA.

tristetraprolin [46,47]. Thus, the dual application of oHA and DOX may present a compelling strategy for TNBC treatment by alleviating chemoresistance and inhibiting immunosuppression.

Our previous work has demonstrated that oHA alone can attenuate phosphorylated ERK1/2 signaling and, when combined with DOX, exerted antitumor and anti-metastasis effects in a xenogeneic TNBC mouse model [48], which is attributable to its effect on reducing cancer cell adhesion, migration, and proliferation through the antagonistic impact of oHA on the HA receptors [48]. In this study, we investigate the synergistic combination of DOX and oHA *co*-delivered by polymer-lipid nanoparticles (PLN) on 1) DNA damage and repair response, 2) PD-L1 expression, and 3) tumor growth and metastasis for both BRCA1-mutant and wild type TNBC mouse models as compared to olaparib treatment, a standard adjuvant therapy for BRCA-mutated TNBC and other solid tumors. To preferentially target TNBC cells and tumor vasculature through their overexpressed αvβ3 and αvβ5 integrins, the iRGD (CRGDK/RGPD/EC)-peptide [49–51] was grafted onto the surface of the NP that are co-loaded with DOX and oHA and referred to as iRGD-DOX-oHA-PLN (Fig. 1, A and B). The efficacy of iRGD-DOX-oHA-PLN in the simultaneous treatment of primary breast tumors and the prevention of spontaneous metastasis was assessed using a murine spontaneous metastasis model of TNBC that closely replicates the clinical manifestation of the disease [52]. The integrin-targeted delivery of both agents significantly improves the nanoformulations accumulation and penetration, facilitating greater tumoral drug accessibility and concentration at the molecular target. The oHA delivered to the tumors enhanced the sensitivity of tumors to DOX toxicity and demonstrated a synergistic cytotoxic effect that significantly inhibited the growth of primary breast tumors by promoting cancer cell apoptosis likely through the expression reduction in PD-L1, RHAMM, single and double DNA strand repair proteins (PARP1, RAD51, RAD50, and BRCA1), and the increased DNA double-strand breaks, showcasing superior efficacy compared to olaparib. The anti-tumor and anti-metastatic capabilities of iRGD-DOX-oHA-PLN were extensively investigated in both BRCA mutant and wild tumor models, demonstrating its overwhelming impact *in vitro* and *in vivo*.

2. Materials and methods

2.1. Materials

Unless otherwise mentioned, all chemicals were purchased from Sigma-Aldrich Canada (Oakville, ON, Canada). The oHA was purchased from Bloomage Biochem Co., Ltd. (Shandong, China). Cyclic peptide iRGD [c(CRGDRGPDC)] was purchased from LifeTein (Somerset, NJ, USA). DOX HCl and olaparib were purchased from MedChemExpress (Monmouth Junction, NJ, USA). The MDA-MB-231-luc-D3H2LN cell line was purchased from Caliper Life Sciences (Hopkinton, MA, USA). MDA-MB-436 and MCF10A were purchased from Cedarlane (Burlington, ON, Canada). The suppliers confirmed that all cell lines were pathogen-free by using polymerase chain reaction (PCR) techniques. The anti-poly(ADP-ribose) (anti-PAR) (79109S) antibody and anti-RHAMM antibody (sc-515,221) were purchased from Santa Cruz (Toronto, ON, Canada), and the following antibodies: anti-β-actin (ab8226), anti-H2AX (ab26350), anti-PARP1 (ab32138), anti-RAD51 (ab133534), anti-RAD50 (ab89), anti-PD-L1 (ab205921), anti-BRCA1 (ab16780) were purchased from Abcam (Mississauga, ON, Canada).

2.2. Preparation and characterization of nanoparticles

DOX and oHA *co*-loaded polymer lipid nanoparticles (DOX-oHA-PLN) were prepared using a self-assembly method [53,54]. Briefly, to a lipid-polymer mixture of 25 mg of ethyl arachidate, 2 mg of Myrj52 (PEG40SA), and 1 mg Myrj59 (PEG100SA), which is preheated to 60 °C, oHA (100 μL, 100 mg mL^{-1}), DOX (250 μL, 10 mg mL^{-1}), and Pluronic® F-68 (PF 68, 50 μL, 100 mg mL^{-1}) in distilled deionized (DDI) water were added and stirred for 20 min. The suspension was emulsified at 60 °C at 100 % peak power for 5 min using a Hielscher UP 100H probe ultrasonicator (Ringwood, NJ, USA), followed by a quick emulsion transfer into 2.1 mL of saline or 5 % dextrose being stirred on ice to generate DOX-oHA-PLN. For *in vivo* injections, saline was used to prepare the formulations, whereas phosphate-buffered saline (PBS) was used for *in vitro* treatments.

To synthesize iRGD-conjugated DOX-oHA-PLN (iRGD-DOX-oHA-PLN), Myrj59-iRGD, synthesized and characterized as previously described [54,55], was used instead of unconjugated Myrj59 followed by the same NP preparation process. Nanoparticles without DOX, or both DOX and oHA (oHA-PLN, iRGD-oHA-PLN, or iRGD-PLN) were prepared by the same method without the DOX solution or oHA solution. The size and zeta potential of the particles were determined using a Malvern Zetasizer Nano ZS (Worcestershire, UK). For the synthesis of NPs without oHA (DOX-PLN, iRGD-DOX-PLN), a hydrolyzed epoxidized soybean oil polymer (HPESO) [56] was used to complex with DOX in place of oHA. For fluorescent detection, iRGD-oHA-PLN and oHA-PLN nanoparticles were conjugated with cyanin 5 (Cy5) linked to oHA. This modification facilitated the visualization of iRGD-NPs when bound to αvβ3-integrin, which was coated onto the wells of a 96-well plate.

2.3. Maintenance of cell culture

Human MDA-MB-231-luc-D3H2LN cells were cultured in α-modified minimal essential medium (α-MEM) supplemented with 10 % fetal bovine serum (FBS) and maintained at 37 °C in a humidified incubator with a 5 % CO_2 atmosphere. This culture environment was facilitated using cell culture flasks supplied by Corning (Corning, New York, U.S.A.), and the growth medium were procured from Gibco-Life Technologies (Burlington, ON, Canada) for α-MEM and Invitrogen Inc. (Burlington, ON, Canada) for FBS.

MDA-MB-436 cells were cultivated in Dulbeccos Modified Eagles Medium (DMEM) enriched with sodium pyruvate and 10 % FBS. These cells were also incubated at 37 °C in a humidified atmosphere containing 5 % CO_2, with the medium components sourced from Wisent Inc. (ST-BRUNO, Quebec, Canada).

MCF10A cells, obtained from the ATCC, were grown under similar conditions at 37 °C and 5 % CO_2. The culture medium for these cells was the Mammary Epithelial Cell Growth Medium BulletKit™ from Lonza (MEGM, CC-3150, Mississauga, Canada), specifically designed for mammary epithelial cell growth. This medium was supplemented with cholera toxin (100 ng mL^{-1}) from Cayman (Ann Arbor, MI, USA), human epidermal growth factor (h-EGF-β), recombinant human insulin, hydrocortisone, bovine pituitary extract (BPE), and 5 % heat-inactivated horse serum, with the latter components sourced from Gibco.

2.4. Animal models

The implementation of tumor inoculation, treatment protocols, and euthanasia procedures were conducted in strict accordance with the ethical standards and legal mandates outlined by the Ontario Animals for Research Act and the guidelines of the Federal Canadian Council on Animal Care. These protocols received approval from the University Health Network (UHN) Animal Care Committee under the Animal Use Protocol number 4333.10, UHN, Toronto, ON, Canada.

In the establishment of a spontaneous metastasis model for triple-negative breast cancer, 1×10^6 bioluminescent luciferase-expressing MDA-MB-231-D3H2LN human breast cancer cells were orthotopically implanted into the right inguinal mammary fat pad of 7-week-old female NRG mice. These mice were acquired from the UHN Animal Resource Centre (ARC), with the specific strain being (NOD.Cg-Rag1tm1Mom Il2rgtm1Wjl/SzJ Stock number 007799) (Ontario Cancer Institute, Toronto, ON, Canada). For the development of the MDA-MB-436 orthotopic breast cancer model, the same breed of NRG mice was used, into which cells were inoculated at a concentration of 3.5×10^6,

following identical ethical and procedural guidelines to ensure consistency and reliability in the experimental outcomes.

2.5. In vitro viability and synergy studies

The MDA-MB-436 cells were seeded at a density of 10,000 cells per well in 200 μL of DMEM growth medium using 96-well plate (R and D Systems, Minneapolis, MN, USA) and allowed to culture overnight. To identify the optimal oHA to DOX mass ratio for treatment, the cells were exposed to a fixed DOX concentration (0.1 μg mL^{-1}) in combination with oHA at predetermined oHA:DOX mass ratios of 1:1, 2:1, 4:1, 6:1, 8:1, and 10:1 and incubated for a 24-h period. Cell viability was determined using a SpectraMax M2 microplate reader with the 3-(4,5-dimethylthiazol-2-yl)-2,5-diphenyltetrazolium bromide (MTT) assay (San Jose, CA, USA) at 540 nm. The mass ratio was then fixed at 1:4 in the formulations containing DOX and oHA combinations for subsequent *in vitro* and *in vivo* studies.

The MTT assay was also used to evaluate the synergism of DOX and oHA and the cytotoxicity of iRGD-DOX-oHA-PLN. MDA-MB 231-luc-D3H2LN or MDA-MB-436 cells were plated at a density of 10,000 cells per well in 200 μL of growth medium in 96-well plates overnight. The cells were then treated for 24 h with the free solution or nanoparticle formulation of DOX, oHA, or DOX/oHA combinations with a range of [DOX] of 0.01–50 μg mL^{-1} or [oHA] of 0.04–200 μg mL^{-1}. After being washed three times with PBS, the cells were incubated in a growth medium with the MTT solution for 4 h. The viability was determined using a SpectraMax M2 microplate reader. The median effect analysis was performed to generate the median effect plot and CI based on the cytotoxicity curves of DOX and oHA alone or in combination, free or encapsulated as previously described [48,57,58]. CI values of 1, equal to 1, and greater than 1 indicate synergism, additive effect, and antagonistic impact, respectively.

In addition, cells were seeded in 24-well plates and treated with free DOX, iRGD-DOX-PLN, and iRGD-DOX-oHA-PLN at low DOX concentrations of 0.01 or 0.1 μg mL^{-1} over 72 h and stained with crystal violet.

The viability of MCF10A cells was assessed after being treated with oHA-PLN, DOX-PLN, DOX-oHA-PLN, and iRGD-DOX-oHA-PLN evaluated by MTT. To analyze the effectiveness of each treatment, the viability data were subjected to nonlinear regression analysis utilizing the "Dose-response curves - Inhibition" model with the equation "[Inhibitor] vs. response". This approach was employed within GraphPad software to fit the viability data and calculate the half-maximal inhibitory concentration (IC50) for each treatment condition.

2.6. Drug cellular uptake studies and drug resistance protein

To establish cellular drug uptake profiles, cells were plated onto 96-well plates at a density of approximately 10,000 cells/well at 37 °C. When cells reached 80 % confluency, free DOX/oHA, DOX-oHA-PLN or iRGD-DOX-oHA PLN suspensions were added to each well to evaluate cellular drug accumulation. All treatments were fixed to 15 mg mL^{-1} DOX concentration. At predetermined time intervals ($0-2h$), the supernatant was removed, and cells were washed with ice-cold PBS (pH 7.6) and lysed with PBS containing 0.5 % Triton X-100. DOX concentrations in the cell lysates were transferred to a 96 black-well plate to be measured with SpectraMax Gemini XS microplate fluorometer (Molecular Devices, Sunnyvale, CA) at an excitation wavelength of ex 480 nm and an emission wavelength of em 590 nm. A standard curve with known concentrations of DOX was used to evaluate its presence in the cell lysate. Cellular DOX uptake is expressed as a concentration of micromoles per milligram of protein for each cell line. Protein concentrations of the cell lysates were determined by the bicinchoninic acid assay (BCA) colorimetric assay (Thermo Scientific, Waltham, MA, USA), and bovine serum albumin from the assay kit was used for the protein standard curve determination. *In vitro* DOX uptake was also evaluated in different DOX formulations in MDA-MB-231-luc-D3H2LN and MDA-MB-436 cells with confocal fluorescence laser microscopy for internalized free drugs and nanoparticles in one hour of treatment after cells were plated onto confocal dish at densities of approximately 200,000 cells.

To evaluate the P-gp drug efflux expression with Western blot, MDA-MB-231-luc-D3H2LN cells were cultured in flasks until reaching ~80 % confluency. Cells were treated with saline, free DOX, iRGD-DOX-PLN, and iRGD-DOX-oHA-PLN ([DOX] = 3.5 μg mL^{-1}) for 24 h. Protein expression of P-gp was evaluated by Western blot. Image Lab software quantified the Relative P-gp expression level and normalized to β-actin expression.

To evaluate the P-gp drug efflux expression with confocal fluorescence laser microscopy, MDA-MB-231-luc-D3H2LN cells were seeded in confocal dishes at 2.5×10^5 cells per well overnight for attachment. Cells were treated with saline, free DOX, iRGD-DOX-PLN, and iRGD-DOX-oHA-PLN ([DOX] = 3.5 μg mL^{-1}) for 6 h. Cells were then fixed with 4 % paraformaldehyde (pH 7.4), permeated with 0.1 % Triton X, and stained with Hoechst 33342 before being observed using a confocal microscope.

2.7. Western blotting for measuring DNA damage and repair biomarkers

MDA-MB-231-luc-D3H2LN or MDA-MB-436 cells were cultured in until they reached ~80 % confluency. After cells were treated for 4 h or 24 h, cell extracts were obtained using Radioimmunoprecipitation assay buffer (RIPA buffer) lysis buffer supplemented with protease and phosphatase inhibitors (Thermo Scientific, Waltham, MA, USA). The extracted protein amounts were determined by the Pierce™ B.C.A. Protein Assay Kit (Thermo Scientific), and protein samples were heated at ~95 °C for ~5 min before being separated by electrophoresis in gradient polyacrylamide gels (4–12 %) and transferred to polyvinylidene difluoride (PVDF) membranes (Bio-Rad, Hercules, CA, USA). Following 1 h blocking with 5 % bovine serum albumin (BSA), the PVDF membranes were incubated with the primary antibody of interest or anti-β-actin antibody (Abcam, Mississauga, ON, Canada) at 4 °C overnight. Following washing, the membranes were incubated for 1 h with secondary antibodies before reacting with a luminol-based enhanced chemiluminescence horseradish peroxidase substrate. The images were captured by ChemiDoc™ MP Imaging System and analyzed by Image Lab Software (Bio-Rad, Hercules, CA, USA). The band intensities of the protein bands of interest were normalized to the β-actin band intensity, represented as a ratio from the treated groups, and compared to saline-treated groups.

2.8. iRGD-DOX-oHA-PLN versus olaparib in vitro

MDA-MB-231-luc-D3H2LN or MDA-MB-436 cells were treated with saline, 10 μM olaparib, Free-DOX or iRGD-DOX-oHA-PLN (2 mg/L of DOX) and stained with anti-PAR1 antibody to measure the PARP-1 enzymatic activity. Western blotting was performed after the MDA-MB-231 or MDA-MB-436 cells were treated with olaparib (10 μM) or iRGD-DOX-oHA-PLN (2 mg/L of DOX) and incubated for 24 h using anti-PD-L1 antibody and anti-β actin antibody. In another experiment, PD-L1 staining was evaluated using a confocal laser microscope with the same treatment groups: saline, 10 μM olaparib, or 2 mg/L of iRGD-DOX-oHA PLN for 24 h and stained with anti-PD-L1.

2.9. Immunohistochemical staining of primary tumors

Treatment commenced three weeks following the inoculation of cancer cells, once the tumors had attained a volume of 200 mm^3. The breast tumor-bearing mice were i.v. injected through the tail vein with the following treatments: saline, free DOX, free DOX-oHA, iRGD-DOX-PLN or iRGD-DOX-oHA-PLN with 10 mg kg^{-1} DOX dose and its equivalence of 1:4 when oHA was included. The primary breast tumors were resected 24 h after treatment and fixed with 10 % buffered formalin. Breast tumors were sectioned and stained with human anti-RHAMM,

anti-RAD51, anti-BRCA1 and anti-γH2AX antibodies. The tissue sectioning and staining were performed at the CFIBCR Histology/Microscope Core Unit, Toronto, ON, Canada.

2.10. In vivo efficacy and lung metastasis studies

When breast tumors reached ~150 mm^3 at ~2 weeks after tumor cell injection, the breast tumor-bearing mice were treated by i.v. injection of the following preparations: Group 1 received saline; Group 2 received two doses of iRGD-DOX-oHA-PLN (10 mg kg^{-1} DOX) on day 0 and day 14; and Group 3 received olaparib administered intraperitoneally (i.p.) at a concentration of 50 mg kg^{-1} with five i.p. injections per week (Monday through Friday) over four weeks. The breast tumor size was monitored weekly using calipers, and the following equation: tumor size = (width^2 × length)/2 was used to evaluate tumor volume.

The spontaneous metastases to the lungs and lymph nodes were monitored weekly by detecting the tumor bioluminescence using a Xenogen imager (Caliper Life Sciences, Hopkinton, MA, USA) 10 min after D-luciferin i.p. injections (15 mg kg^{-1}). At week 4, distal metastases were examined by resecting major organs for bioluminescence imaging. Lungs, livers and major organs immediately fixed in 10 % buffered formalin and coronally sectioned and stained with hematoxylin and eosin (H and E) (The Campbell Family Institute for Breast Cancer Research, Ontario Cancer Institute, University Health Network). The metastasis area index quantified the dark purple metastatic nodules in the H and *E*-stained lungs and livers, and metastasis was calculated as the ratio of metastasis area to the total lung or liver area. For staining quantification, the areas were analyzed using HALO™ Image analysis software (PerkinElmer, Waltham, MA, USA).

2.11. Statistical analysis

All quantitative data are presented as mean ± standard deviation (SD). Students *t*-test or one-way analysis of variance (ANOVA) followed by Tukeys posthoc test was utilized to determine statistical significance between two or more groups, respectively. All statistical tests were done in GraphPad Prism Software (Chicago, IL, USA). *P* values <0.05 were considered significant.

3. Results

3.1. The iRGD-DOX-oHA-PLN formulation properties

Nanoparticles were synthesized by ultrasonication of microemulsions in the presence of Pluronic F-68 (PF-68), a non-ionic surfactant, as shown in Fig. 1A. The NPs were measured by dynamic light scattering demonstrating a well-ordered size distribution of ~190–200 nm for both iRGD-oHA-PLN and iRGD-DOX-oHA-PLN (Fig. S1A). iRGD-functionalized nanoparticles were then examined for their ability to bind to recombinant integrin receptors in an *in vitro* binding assay. As shown in Fig. S1B, substantially higher cyanine-5 (Cy5) fluorescence was observed in wells treated with iRGD NPs than in those without the iRGD peptide. A fixed drug-to-polymer mass ratio of 1/4 (DOX/oHA μg mL^{-1}) was chosen, which provided the greatest drug combination cytotoxicity against MDA-MB-436 TNBC cells (Fig. S1C). The size, polydispersity index (PDI) and zeta-potential of various PLN formulations prepared and evaluated for this work is summarized in Fig. S1D.

3.2. The iRGD-DOX-oHA-PLN demonstrated synergy and selectivity for TNBC

The potentiation of DOX activity by oHA was investigated in MDA-MB-231-luc-D3H2LN (BRCA1-wildtype) and MDA-MB-436 (BRAC1-mutant) cells following treatments with oHA-PLN, DOX-PLN, or DOX-oHA-PLN or equivalent concentration of the free drug. Dose-response curves demonstrated higher cytotoxicity of DOX-oHA-PLN compared to free DOX in both cell lines, corresponding to a ~ 5- and 11-fold decrease of the IC50 in MDA-MB-231-luc-D3H2LN and MDA-MB-436, respectively (Fig. 2, Fig. S2, Table S1). The median effect plot and combination index (CI) analysis were calculated based on the dose-response curves of the tested formulations. The results demonstrated a potentiating effect of DOX in combination with oHA when encapsulated in nanoparticles, with a CI below 1 for fractions of affected cells for both cell lines (Fig. 2, A and B bottom panels, and Fig. S2 for free drugs). In addition, iRGD-DOX-oHA-PLN demonstrated prominent growth inhibition for both cell lines following 48 h treatment compared to free DOX or iRGD-DOX-PLN (Fig. S3). This was compared to treatment with olaparib for 24 h in MDA-MB-436 (BRCA-mutant) contrasted with MDA-MB-231-luc-D3H2LN (BRCA1-wild type), as shown in Fig. 2C demonstrating the relative enhancement of cellular cytotoxicity of iRGD-DOX-oHA-PLN.

The MCF10A human mammary epithelial cell line is widely utilized as an *in vitro* model for investigating the functions of non-cancerous breast cells and their transformation processes [59]. Treatment of MCF10A cells with DOX-containing formulations resulted in similar IC50 values, with a marginal enhancement in toxicity observed for the iRGD-DOX-oHA-PLN formulation, as shown by the dose-response curves (Fig. 1D) and IC50 values summarized in Fig. 2E and Table S1. IC50 values obtained for iRGD-DOX-oHA-PLN demonstrate that non-tumorigenic MCF10A cells exhibit IC50 values ~6- and ~ 11-fold higher than those observed for the MDA-MB-231-luc-D3H2LN and MDA-MB-436 TNBC cell lines, respectively. These data suggested a preferential selectivity of iRGD-DOX-oHA-PLN towards TNBC cell lines (Fig. 2E). This selectivity might be due to the poor expression of HA receptors and αvβ3 integrins in the MCF10A [60,61] to be targeted by the iRGD-DOX-oHA-PLN.

3.3. The iRGD-functionalized PLN increased DOX intracellular uptake

To assess the cellular uptake of various formulations, confocal laser scanning microscopy (CLSM) was used to localize fluorescence signals from DOX and oHA-Cy5 in MDA-MB-231-luc-D3H2LN (Fig. S4A) and MDA-MB-436 cells (Fig. S4B), following a one-hour incubation period with free DOX-oHA, DOX-oHA-PLN, and iRGD-DOX-oHA-PLN formulations. Cells treated with iRGD-DOX-oHA-PLN exhibited enhanced uptake of DOX and oHA-Cy5 compared to cells subjected to other treatment modalities. The focal nuclear localization of DOX in these cells suggests that DOX was successfully released from nanoparticles into the cytoplasm for ultimate delivery to the nucleus. Spectrofluorometric analysis of the cellular uptake of various DOX formulations revealed that cells treated with iRGD-DOX-oHA-PLN demonstrated the highest level of DOX accumulation. This was followed by cells treated with DOX-oHA-PLN, with the lowest accumulation observed in cells treated with free DOX-oHA (Fig. S4, C and D).

For MDA-MB-231-luc-D3H2LN cells treated with iRGD-DOX-oHA-PLN for 24 h, there was also a notable reduction in the expression of P-gp compared to cells treated with iRGD-DOX-PLN and free DOX (Fig. S4E). Likewise, treatment of MDA-MB-231-luc-D3H2LN cells with iRGD-oHA-PLN resulted in a significant reduction in the expression of RHAMM compared to cells treated with other oHA formulations (Fig. S5).

3.4. The iRGD-DOX-oHA-PLN induced DNA damage and inhibited DNA repair in vitro

In both BRCA-wild type MDA-MB-231-luc-D3H2LN cells and BRCA-mutant MDA-MB-436 cell lines treatment with DOX significantly elevated DSBs, as indicated by increased expression of γH2AX, when compared to the effects observed with oHA treatment alone (Fig. 3). The co-delivery of oHA with DOX further amplified this effect, with γH2AX upregulation occurring in the following manner: iRGD-DOX-oHA-PLN exhibited the most substantial increase followed by DOX-oHA-PLN, then DOX-oHA, and finally DOX alone which demonstrated the lowest

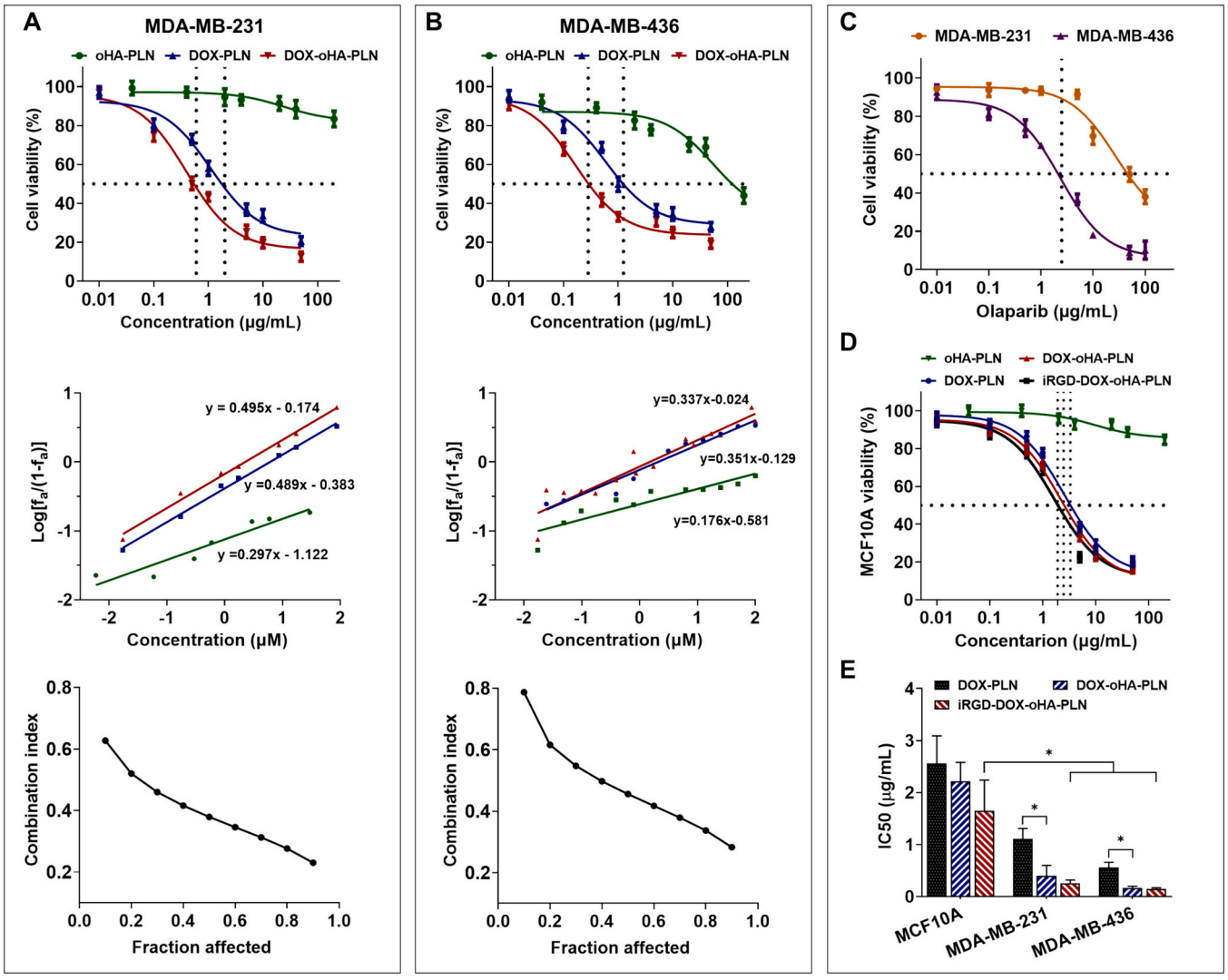

Fig. 2. The potentiating effects of DOX and oHA in enhancing cellular cytotoxicity compared to olaparib in BRCA-wild type and BRCA-mutant cell lines. Dose-response curve of cell viability (IC50 values shown by dotted lines) of MDA-MB-231-luc-D3H2LN (A) and MDA-MB-436 (B) treated with oHA-PLN, DOX-PLN, or DOX-oHA-PLN (at a DOX/oHA mass ratio of 1:4) for 24 h (top plots). The middle plots are the median effect plots (Log[f_a/(1-f_a)]), and the bottom plots are combination index analyses. (C) Dose-response curves of MDA-MB-231-luc-D3H2LN and MDA-MB-436 cell lines treated with olaparib for 24 h. (D) Dose-response curve of the non-malignant breast epithelial MCF10A cells treated with oHA-PLN, DOX-PLN, DOX-oHA-PLN, and iRGD-DOX-oHA-PLN (at DOX:oHA ratio of 1:4) for 24 h. (E) Fold change comparisons of IC50 values of MCF10A, MDA-MB-231-luc-D3H2LN, and MDA-MB-436 after nanoparticle treatment. Data are presented as mean ± SD ($n = 3$). *$p < 0.05$.

level of enhancement. Administration of oHA mitigated DOX-induced upregulation of DNA repair proteins RAD50, RAD51, and PARP1. The most significant attenuation was observed in cells treated with iRGD-DOX-oHA-PLN, followed by those treated with DOX-oHA-PLN, and the least pronounced effect was seen in cells treated with free DOX-oHA (Fig. 3, A and B).

3.5. *The iRGD-DOX-oHA-PLN reduced DNA break repair without increasing PD-L1 expression*

Levels of RAD51 and γH2AX foci in MDA-MB-231-luc-D3H2LN cells were visualized using CLSM following treatment with different formulations of oHA alone, DOX alone, or a combination of both. oHA formulations demonstrated a reduction in RAD51 foci, with an approximately 8-fold decrease in the percentage area of stained foci in cells treated with iRGD-oHA-PLN compared to saline (Fig. 4A). Treatment with free DOX resulted in an induction of RAD51 expression. By contrast, iRGD-DOX-oHA-PLN treatment demonstrated a 5-fold decrease in RAD51 expression compared to free DOX. Similarly, there was a two-fold increase in γH2AX staining intensity following treatment with iRGD-DOX-oHA-PLN compared to free DOX, indicating significantly enhanced levels of DNA damage (Fig. 4A) consistent with results of Western analyses (Fig. 3, A and B). For comparison, MDA-MB-231-luc-D3H2LN and MDA-MB-436 cells underwent treatment with saline, olaparib, free DOX, and iRGD-DOX-oHA-PLN and were analyzed by Western analysis for γH2AX, RAD50, RAD51, and PARP1. Contrary to the effects of free DOX, both olaparib and iRGD-DOX-oHA-PLN resulted in a decrease in PARP1. This outcome was also evidenced by the faint presence of poly-ADP ribose chain bands in the Western blots of both cell lines (Fig. S6, A and B). Notably, only iRGD-DOX-oHA-PLN treatment led to a robust reduction in RAD50 and RAD51 expression compared to the reductions observed with olaparib and free DOX treatments, as shown in Fig. 4B and C.

PARP1 inhibitors, such as olaparib, have been shown to elevate PD-L1 expression, contributing to an immunosuppressive TME [62]. Therefore, the impact of iRGD-DOX-oHA-PLN on PD-L1 protein expression was evaluated and compared to olaparib. Cells were treated with either iRGD-DOX-oHA-PLN or olaparib, followed by CLSM and

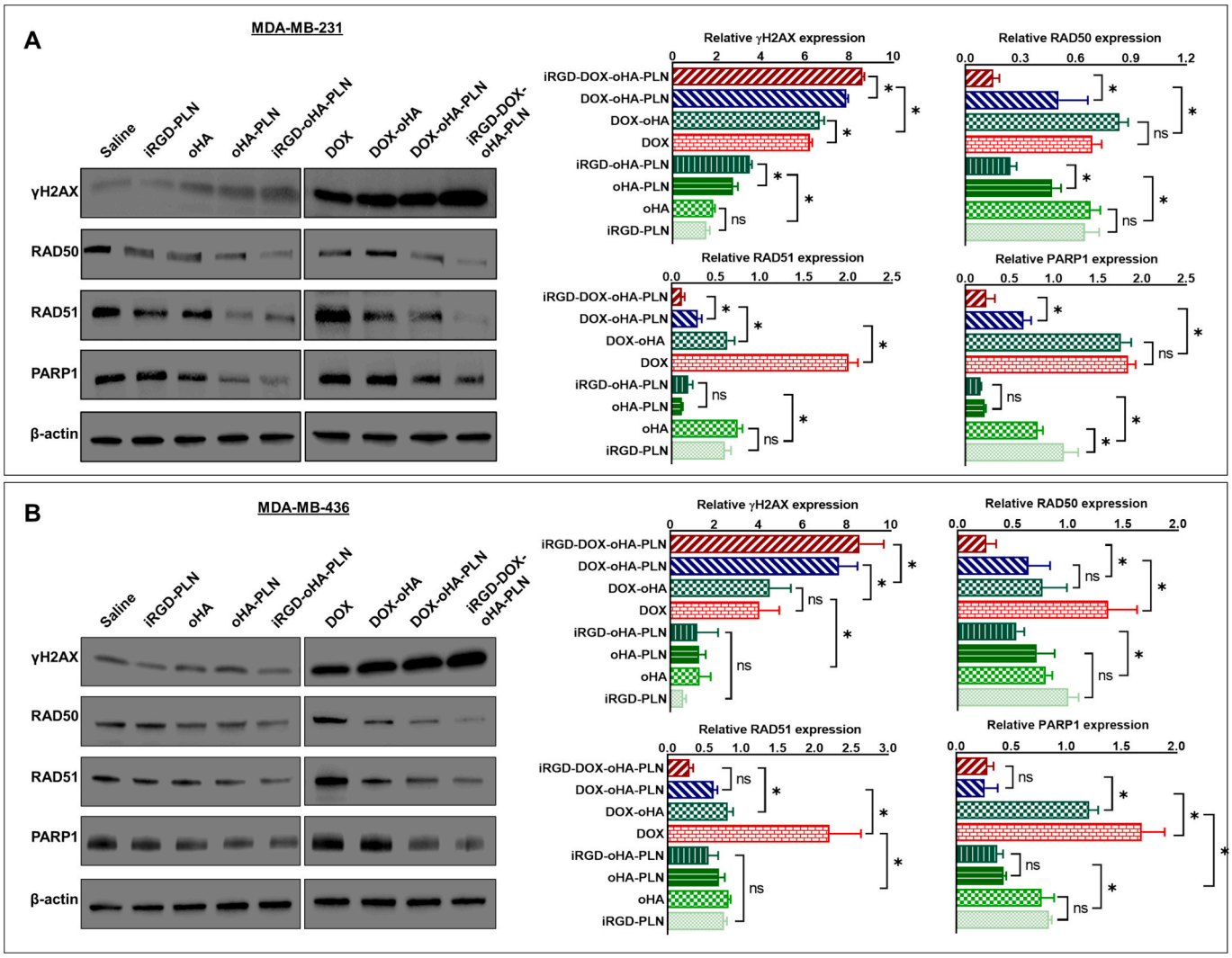

Fig. 3. IRGD-DOX-oHA-PLN inhibited DNA repair and promoted DNA damage in both BRCA-wild type and BRCA-mutant cells. (A) Expression of γH2AX, RAD50, RAD51, and PARP1 in MDA-MB-231-luc-D3H2LN cells, (B) MDA-MB-436 cells following 4 h of treatment with different formulations (saline, iRGD-PLN, free-oHA, oHA-PLN, iRGD-oHA-PLN, free-DOX, DOX-oHA-PLN, and iRGD-DOX-oHA-PLN). Right panels represent the quantitative analysis of band intensities normalized to β-actin and normalized against respective saline-treated groups. Data are presented as mean ± SD ($n = 3$). *$p < 0.05$.

immunoblotting to assess PD-L1 expression levels. These experimental approaches yielded similar outcomes, demonstrating that olaparib treatment induced PD-L1 expression, whereas iRGD-DOX-oHA-PLN treatment resulted in a notable reduction of PD-L1 expression. This was evidenced by diminished PD-L1 fluorescence staining in the CLSM images and faint bands in the Western blot images. (Fig. 4, D and E).

3.6. The iRGD-DOX-oHA-PLN enhanced DNA damage and suppressed DNA repair in vivo

Orthotopic human MDA-MB-231-luc-D3H2LN and MDA-MB-436 breast cancer transplant models were utilized to examine nanoparticle effects on expression levels of RHAMM and DNA damage-related proteins in primary tumors collected 24 h post-treatment. Immunohistochemical (IHC) analysis revealed significant reductions in RHAMM expression in both MDA-MB-231-luc-D3H2LN and MDA-MB-436 breast tumor models in the order of iRGD-DOX-oHA-PLN (13.6 % and 6.8 %) < DOX-oHA (28.48 % and 13.2 %) < iRGD-DOX-PLN (65.0 % and 39.5 %) < DOX (68.9 % and 50.2 %) < saline (80.7 % and 64.8 %) (Fig. 5). The decrease in RHAMM expression mediated by iRGD-DOX-oHA-PLN and iRGD-DOX-PLN treatments corresponded to an approximately 4.9-fold and 8.5-fold reduction respectively in MDA-MB-231-luc-D3H2LN and MDA-MB-436 tumors transplants. IHC analysis supported Western blot results, demonstrating decreased RAD51 expression in MDA-MB-231-luc-D3H2LN and MDA-MB-436 models treated with iRGD-DOX-oHA-PLN, with expression levels at 42.3 % and 21.2 % of saline controls, respectively. This represented a marked reduction compared to that induced by DOX alone, 134 % for MDA-MB-231-luc-D3H2LN and 156.4 % for MDA-MB-436 tumors, respectively. (Fig. 5). In addition, expression of γH2AX significantly increased following treatment with iRGD-DOX-oHA-PLN, with the percentage of positive cells rising from approximately 10 % in the DOX-treated groups to 37.7 % in MDA-MB-231-luc-D3H2LN tumors and 46.6 % in MDA-MB-436 tumors (Fig. 5). Notably, a significant reduction in BRCA1 staining was observed exclusively in MDA-MB-231-luc-D3H2LN tumors treated with oHA-containing formulations. The reduction was marked, with approximately 25.2 % in the DOX-oHA group and about 6.8 % in the iRGD-DOX-oHA-PLN group, compared to ~36–40 % in the saline, DOX, and iRGD-DOX-PLN treated groups (Fig. 5A). In the BRCA1-mutant MDA-MB-436 tumor model, BRCA1 expression underwent only slight changes as these cells lack BRCA1 (Fig. 5B).

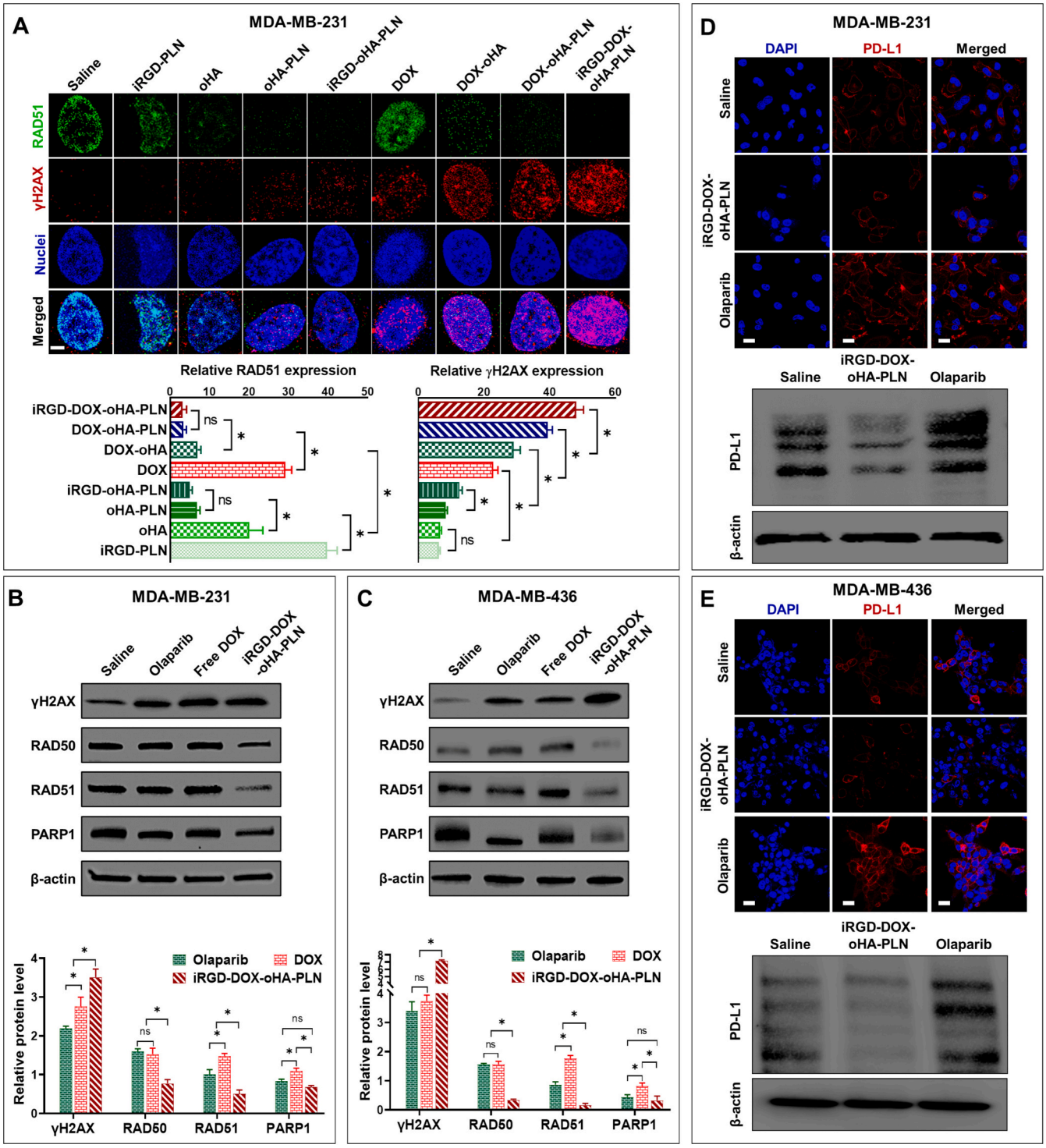

Fig. 4. iRGD-DOX-oHA-PLN suppressed DNA repair without inducing PD-L1 expression. (A) Representative CLSM images of MDA-MB-231-luc-D3H2LN cell nuclei staining for RAD51 (green), γH2AX (red), and nuclear DNA (blue) following saline, iRGD-PLN, free oHA, oHA-PLN, iRGD-oHA-PLN, free DOX, DOX-oHA, DOX-oHA-PLN, and iRGD-DOX-oHA-PLN treatment for 4 h. Scale bar = 20 μm. Foci were calculated based on the area of γH2AX or RAD51 foci within the nucleus. Data are presented as mean ± SD. $n = 3$. *$p < 0.05$. (B and C) Representative Western blots of γH2AX, RAD50, RAD51, and PARP1 expression in MDA-MB-231-luc-D3H2LN cells and MDA-MB-436 cells after different treatments (saline, olaparib, DOX, and iRGD-DOX-oHA-PLN) for 4 h. Band intensity was normalized to their respective β-actin loading controls and respective saline-treated groups. Scale bar = 50 μm. Data are presented as mean ± SD. n = 3. *p < 0.05. (D and E) Representative CLSM images and Western blots of PD-L1 expression in MDA-MB-231-luc-D3H2LN and MDA-MB-436 cells treated for 24 h Cells were treated with saline, olaparib (10 μM) or iRGD-DOX-oHA-PLN (2 mg/L of DOX).

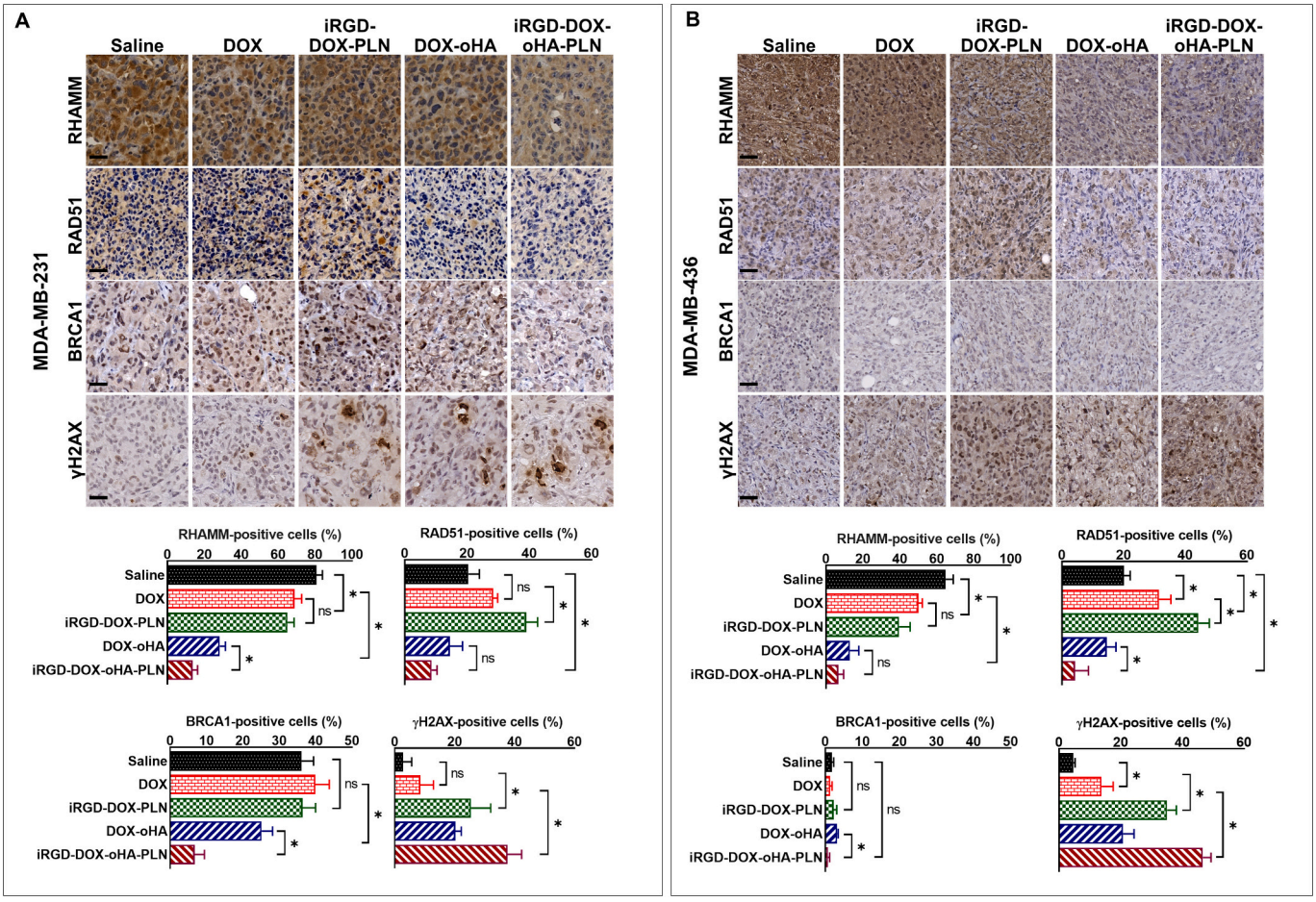

Fig. 5. *In vivo* targeted delivery of DOX / oHA combination prevented DNA repair, inducing DNA damage in human MDA-MB-231-luc-D3H2LN and MDA-MB-436 cells. (A and B Top panels) Representative images of the IHC staining of RHAMM, RAD51, BRCA1, and γH2AX in MDA-MB-231-luc-D3H2LN and MDA-MB-436 breast cancer model tumor sections after the treatment with saline, free DOX, iRGD-DOX-PLN, free DOX-oHA, or iRGD-DOX-oHA-PLN. All treatments were formulated at a DOX concentration of 10 mg kg^{-1}. Scale bar = 50 μm. (A and B Bottom panels) Quantification of the entire tissue sections stained with antibodies specified in the top panels. Data are presented as mean ± SD. $n = 3$. *$p < 0.05$.

3.7. The iRGD-DOX-oHA-PLN prevented tumor growth and inhibited development of lung and liver metastases

As shown in Fig. 6A, both olaparib and iRGD-DOX-oHA-PLN were examined for therapeutic effectiveness in preventing spontaneous lung and liver metastases in orthotopic MDA-MB-231-luc-D3H2LN or MDA-MB-436 tumor-bearing NRG mice. For MDA-MB-231-luc-D3H2LN tumor-bearing mice, the lung was continuously monitored for metastases *via* bioluminescence imaging over four consecutive weeks. According to *in vivo* bioluminescence imaging data, metastatic occurrences were identifiable in the saline-treated group as soon as the first week and manifested in the olaparib-treated group by the second week, as shown in Fig. 6 B. In contrast, for most animals treated with iRGD-DOX-oHA-PLN, no bioluminescence signal indicating metastatic growth in the lung was detected for up to four weeks. The findings were further corroborated by *ex vivo* bioluminescence imaging of the harvested major organs at the end of treatment, as illustrated in Fig. 6.

The cellular structure of metastatic tumor nodules was further analyzed in lung and liver tissues at week 4, revealing that the iRGD-DOX-oHA-PLN treatment group exhibited the fewest nodules in both tumor models. The quantification of lung and liver metastases through the metastases area index also showed a reduction of metastases in the lungs and livers of the iRGD-DOX-oHA-PLN-treated groups compared to those treated with olaparib. (Fig. 6 C and D, left panels). It was determined that iRGD-DOX-oHA-PLN inhibited tumor growth by approximately 88 % and 64 % compared to saline and olaparib, respectively, in the MDA-MB-231-luc-D3H2LN tumor model. In the BRCA1-mutant MDA-MB-436 tumor model, iRGD-DOX-oHA-PLN achieved inhibition of tumor growth by roughly 89 % and 73 % when compared to saline and olaparib, respectively. Notably, this therapeutic efficacy did not induce significant changes in the body weights of mice across the treatment groups in both TNBC models (Fig. 6 C and D). Fig. 6 E compares the tumor volumes as well as liver and lung metastasis between BRCA1 wild-type (MDA-MB-231) and BRCA1-mutant (MDA-MB-436) tumor models treated with iRGD-DOX-oHA-PLN or olaparib. The data reveal that olaparib is more effective in reducing tumor growth and metastasis in the BRCA1-mutant MDA-MB-436 model compared to the wild-type tumor. In contrast, the iRGD-DOX-oHA-PLN demonstrated equal efficacy in both BRCA1 wild-type and BRCA1-mutant models. After four weeks of treatment, no apparent toxicity was observed in olaparib and iRGD-DOX-oHA-PLN treatment groups (Fig. S7).

4. Discussion

To successfully treat TNBC and prevent relapse and metastases, it is essential to overcome current chemotherapeutic limitations by developing targeted, less toxic and personalized medical treatments that overcome drug resistance and tumor heterogeneity. Overexpression of drug efflux pumps, upregulation of DNA repair proteins, and immune evasion mechanisms significantly contribute to treatment failure in

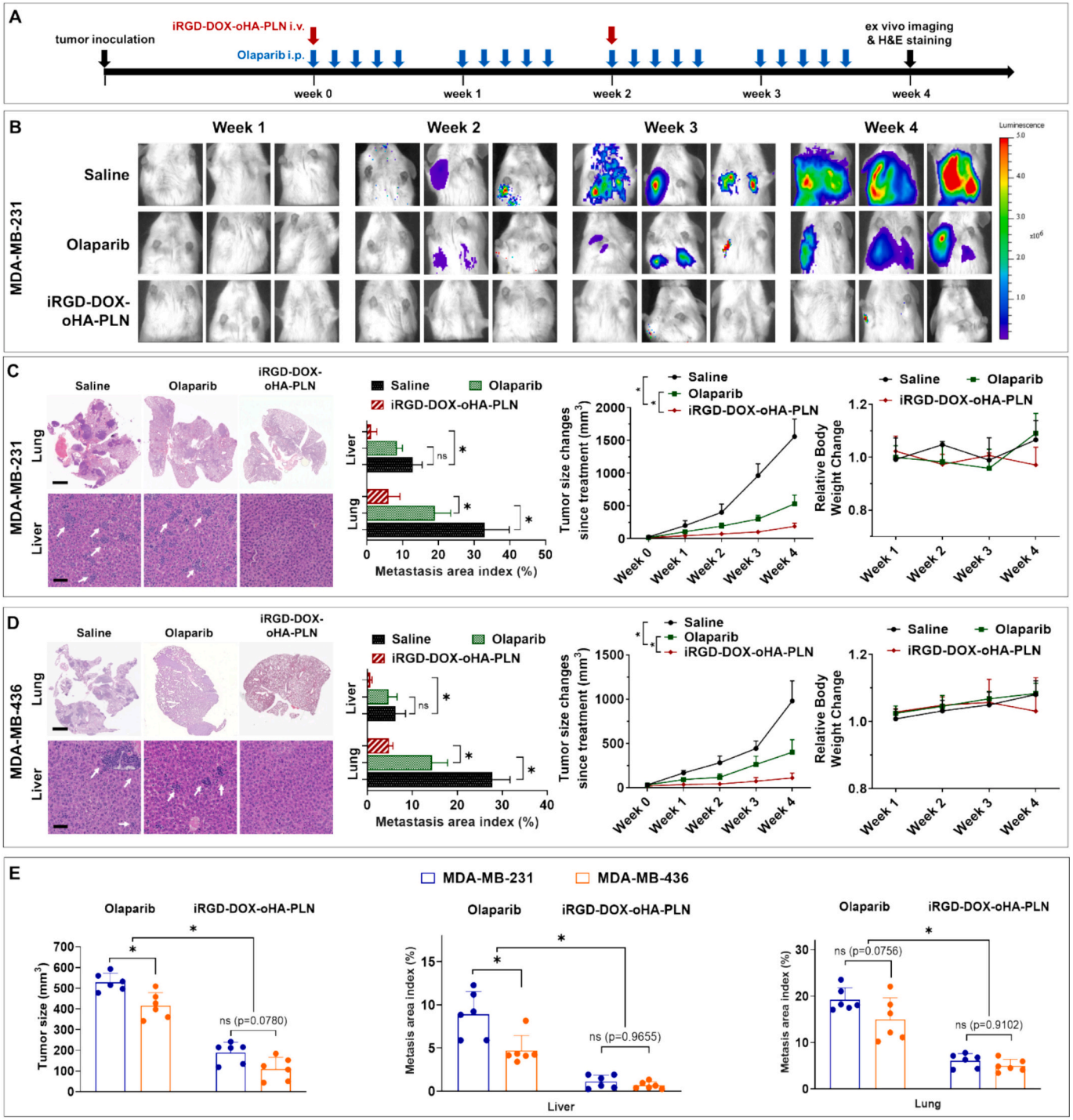

Fig. 6. IRGD-DOX-oHA-PLN prevented lung metastases and tumor progression in TNBC tumors. (A) Schematic of the time frame of experimental procedures performed on orthotopic tumor-bearing mice, including tumor inoculation, iRGD-DOX-oHA-PLN (10 mg kg^{-1} of DOX, i.v. one dose on day 0 and one dose on day 14) or olaparib injections (50 mg kg^{-1}, five i.p. injections/week (Monday to Friday) for a total of 20 injections), and then animals were sacrificed at the endpoint. (B) *In vivo* bioluminescence images of lung metastases progression over four weeks. (C and D, Left Panels) Representative H and E images of lungs and livers harvested from MDA-MB-231-luc-D3H2LN and MDA-MB-436 tumor-bearing mice at week 4 and quantification of metastases area. Metastatic lung and liver nodules were quantified using HALO image analysis software. Scale bar = 100 μm for liver and 1.5 mm for lung H and *E*-stained images. (C and D, Right Panels) The average MDA-MB-231-luc-D3H2LN and MDA-MB-436 tumor sizes and body weights of animals were obtained over 4 weeks. (E) Comparisons of tumor volumes and metastasis area index in the liver and the lungs at week 4 in BRCA1 wild-type (MDA-MB-231) and BRCA1-mutant (MDA-MB-436) tumor models treated with iRGD-DOX-oHA-PLN or olaparib. $n = 6$ for the tumor-bearing animals used per treatment group. Results are presented as mean ± SD. *$p < 0.05$.

TNBC. In this respect, inhibitors of PI3K and MAPK pathways such as Copanlisib and AZD8186 are currently being explored in pre-clinical and clinical settings in conjunction with chemotherapy to counteract tumor drug resistance through modification of the DNA damage response, aiming to replicate the efficacy of PARP inhibitors against HR-defective (BRCA1-mutant) tumors through the principle of synthetic lethality [63–65]. The effectiveness of PARP inhibitors is similarly challenged with the development of drug resistance through the induction of PD-L1

and tumor-associated macrophages, which inhibit cytotoxic T cells from mounting an effective antitumor immune response [64]. The DNA repair machinery plays a crucial role in mediating chemotherapy resistance, particularly within cancer stem cells, and has also been implicated in facilitating metastasis to secondary organs [66,67]. Nuclear proteins such as ataxia telangiectasia mutated (ATM), γH2AX, RAD50, DNA-dependent protein kinase (DNA-PK), RAD51, and BRCA1 serve as flags, mediators, transducers, and effectors in the DNA damage and repair response [68,69].

Based on our previous published work by Zhang et al., the co-encapsulation of DOX and oHA into iRGD-functionalized PLN demonstrated enhanced cellular and tumor uptake of both drugs through integrin and CD44 receptor-targeting [48]. By inhibiting the p-ERK signaling pathway, this formulation effectively reduced the orthotopic breast tumor models primary tumor growth and systemic metastasis [48]. The superior outcomes of the iRGD-DOX-oHA-PLN compared to free drug formulations, including increased apoptosis, reduced toxicity, and enhanced drug accumulation in tumors, which highlights the synergistic combination potential in overcoming the limitations of conventional therapies [48]. In the current study, we are exploring the co-loaded DOX and oHA in iRGD functionalized PLN therapeutic strategy to inhibit the TNBC primary tumor and its metastasis in orthotopic breast tumor murine models of human MDA-MB-231-luc-D3H2LN (BRCA1 wild-type) and MDA-MB-436 (BRCA1-mutant) TNBC cell lines in contrast to olaparib. The rationale behind the efficacy of combining oHA with DOX in iRGD-functionalized PLN is grounded in the hypothesis that oHAs antagonistic action on native HA receptors would disrupt the PI3K/ERK1/2 signaling pathways, consequently modulating the DNA damage response by iRGD-DOX-oHA-PLN treatment in both TNBC tumor models.

The developed iRGD-DOX-oHA-PLN increased cellular uptake of DOX and oHA-Cy5 relative to both unencapsulated drug and non-targeted nanoparticle formulations, attributed to the receptor-mediated endocytosis facilitated by the integrin-targeting capabilities of the iRGD peptide. The confocal microscopy studies revealed dense cytosolic localization and nuclear staining of oHA-Cy5 delivered by the nanoparticles indicating oHAs intracellular bioavailability to participate in signal transduction modifications (Fig. S4). The inhibition of ERK phosphorylation by iRGD-oHA-PLN treatment encouraged us to investigate single and double strand break given the role ERK1/2 phosphorylation plays in activating a PARP1 feedback [70–73]. The process of poly(ADP-ribosyl)ation of proteins known as PARylation, is a PARP1-mediated post-translational modification involving the covalent attachment of ADP-ribose [74]. The formulations containing oHA reduced PARP1 after treatment, as shown in Figs. 3 and 4, B and C. The ability of PARP1 to catalyze the addition of ADP-ribose polymers was evaluated in both MDA-MB-231-luc-D3H2LN and MDA-MB-436 cells (Fig. S6). Both olaparib and the iRGD-DOX-oHA-PLN demonstrated efficacy in inhibiting PARP1 parylation, suggesting these treatments can effectively modulate DNA repair in TNBC cells (Fig. S6, A and B). In addition, iRGD-DOX-oHA-PLN was observed to decrease PD-L1 levels in contrast to olaparib treatment. These findings align with multiple studies indicating that loss of the PTEN (phosphatase and tensin homolog) gene or continuous activation of the PIK3CA genes (encoding the catalytic subunit alpha of phosphatidylinositol-4,5-bisphosphate 3-kinase) activates the PI3K/AKT pathway. Activation of this pathway has been shown to upregulate PD-L1 expression in various cancer isoforms including glioma, breast, and prostate cancers [75–77]. The reduction of PD-L1 induced by iRGD-DOX-oHA-PLN suggests a potential therapeutic advantage by mitigating the immune evasion *via* PD-L1 within the tumor microenvironment.

Incorporating oHA into iRGD-DOX-oHA-PLN nanoparticles significantly modulated DNA damage response, as evidenced by the reduced expression of essential DNA repair proteins RAD51, RAD50, and BRCA1. This resulted in a notable increase in induced DNA DSBs, observed through a marked elevation in γH2AX levels. Specifically, western analysis indicated an enhancement of γH2AX of approximately 8-fold in cells treated with the iRGD-DOX-oHA-PLN compared to those treated with saline, suggestive of a substantial increase in DNA damage (Fig. 3, A and B). In the MDA-MB-231-luc-D3H2LN (BRCA1 wild-type) tumor models, formulations that included oHA led to a notable decrease in BRCA1 expression, as evidenced by BRCA1 staining in Fig. 5A. By contrast, BRCA1 expression levels were not altered in MDA-MB-436 (BRCA1-mutant) tumors by the different treatments, reflecting the inherent absence of BRCA1 expression in these cells. (Fig. 5B BRCA1 staining). The HR pathway, encompassing essential proteins such as BRCA1, RAD51, and RAD50, plays a critical role in high-fidelity DNA repair mechanisms that maintain genomic integrity. This pathway contributes to cancer chemoresistance and the potential for disease relapse, as it enables tumor cells to repair the DNA damage induced by chemotherapy, thereby diminishing the treatment efficacy. Furthermore, our findings emphasize the intricate physical and functional interactions between BRCA1 and RHAMM proteins and their involvement with Aurora Kinase A (AURKA). AURKA is pivotal in organizing cytoskeletal microtubules, regulating a complex network of interactions that contribute to DNA repair and play a significant role in cell division and structural organization within cancer cells [78,79].

Importantly, metastasis in TNBC predominantly targets the lung, liver, bone, and brain [80,81]. The present study demonstrates that the iRGD-DOX-oHA-PLN formulation effectively prevented metastasis to the lung and liver for up to four weeks following treatment. Histological analyses revealed minimal residual disease and significantly reduced metastatic progression. The enhanced therapeutic performance of DOX in this context is attributed to the synergistic effect of co-delivering oHA directly to cancer cells facilitated by the targeting capabilities of the iRGD peptide. This strategy improves drug delivery efficiency and potentially reduces the likelihood of metastatic spread, highlighting the role of formulation in addressing TNBC treatment challenges. Compared to olaparib, the iRGD-DOX-oHA-PLN formulation exhibited comparable efficacy in both BRCA1 wild-type and BRCA1-mutant models, suggesting a wider therapeutic potential independent of BRCA mutation status. This therapeutic efficacy may be attributed to the inhibition of PI3K/AKT and MAPK/ERK signaling pathways downstream of native HA receptors, which likely influences the DNA damage response and modulates tumor immunity. This innovative approach addresses and overcomes numerous challenges associated with the current standard of care, offering a new avenue for effective TNBC therapy through targeted drug delivery, enhanced drug efficacy, and reduced metastatic potential.

5. Conclusion

This study presents a nanoparticulate drug combination strategy using oligomeric hyaluronic acid and doxorubicin encapsulated in polymer-lipid nanoparticles conjugated to an integrin-targeted iRGD-peptide to overcome chemoresistance and immunosuppression in TNBC effectively. The iRGD-DOX-oHA-PLN formulation enhances doxorubicin efficacy by increasing DNA double-strand breaks and reducing PD-L1 expression, thereby inhibiting tumor progression and reducing metastases more effectively than the PARP inhibitor olaparib. This approach disrupts DNA damage repair and drug efflux pathways, providing a comprehensive solution to TNBC challenges. These findings emphasize the potential of nanoparticle-based drug delivery systems in improving therapeutic outcomes and addressing chemoresistance and immune evasion in TNBC, paving the way for strategic and targeted cancer therapy.

Funding

The Canadian Institutes of Health Research grant (Multitargeted Nanomedicine of Synergistic Drug Combinations for Metastatic Breast Cancer Therapy).

CRediT authorship contribution statement

Ibrahim Alradwan: Conceptualization, Methodology, Investigation, Visualization, Supervision, Writing – original draft, Writing – review & editing. **Pei Zhi:** Investigation, Visualization, Writing – review & editing. **Tian Zhang:** Methodology. **HoYin Lip:** Visualization. **Abdulmottaleb Zetrini:** Methodology. **Chunsheng He:** Investigation. **Jeffrey T. Henderson:** Supervision, Writing – review & editing. **Andrew M. Rauth:** Supervision, Writing – review & editing. **Xiao Yu Wu:** Conceptualization, Supervision, Writing – review & editing.

Declaration of competing interest

The authors declare no conflict of interest.

Data availability

All data are available in the main text or the supplementary materials.

Acknowledgments

This work was supported in part by the Canadian Institutes of Health Research. The authors also thank the National Science and Engineering Research Council (NSERC) of Canada for the Equipment Grants to X.Y. Wu; King Abdulaziz City for Science and Technology (KACST) for the scholarship to Ibrahim Alradwan (Advanced Diagnostics and Therapeutics Institute), Ontario Graduate Scholarship (OGS), University of Toronto open scholarship, and top up scholarship from the Graduate Department of Pharmaceutical Sciences to T. Zhang and H. Lip; the Chinese Scholarship Council for the Joint Student scholarship to P. Zhi; and technical contribution in the breast tumor sample processing and immunohistochemistry staining from Dr. Andrew J. Elia, Centre for Integrative Immune Analysis (CIIA) Histology Core, Princess Margaret Cancer Centre (PMH), University Health Network.

Appendix A. Supplementary data

Supplementary data to this article can be found online at https://doi.org/10.1016/j.jconrel.2024.11.061.

References

[1] A. Ignatov, H. Eggemann, E. Burger, T. Ignatov, Patterns of breast cancer relapse in accordance to biological subtype, J. Cancer Res. Clin. Oncol. 144 (2018) 1347–1355.
[2] O. Yersal, S. Barutca, Biological subtypes of breast cancer: prognostic and therapeutic implications, World J. Clin. Oncol. 5 (2014) 412–424.
[3] C.K. Anders, L.A. Carey, Biology, metastatic patterns, and treatment of patients with triple-negative breast cancer, Clin. Breast Cancer 9 (Suppl. 2) (2009) S73–S81.
[4] V. Thakur, R.V. Kutty, Recent advances in nanotheranostics for triple negative breast cancer treatment, J. Exp. Clin. Cancer Res. 38 (2019), 430–430.
[5] S. Mazzucchelli, M. Truffi, F. Baccarini, M. Beretta, L. Sorrentino, M. Bellini, M. A. Rizzuto, R. Ottria, A. Ravelli, P. Ciuffreda, D. Prosperi, F. Corsi, H-ferritin-nanocaged olaparib: a promising choice for both BRCA-mutated and sporadic triple negative breast cancer, Sci. Rep. 7 (2017) 7505.
[6] A. Fabi, L. Carbognin, A. Botticelli, I. Paris, P. Fuso, M.C. Savastano, N. La Verde, C. Strina, R. Pedersini, S. Guarino, G. Curigliano, C. Criscitiello, M. Raffaele, A. Beano, A. Franco, M.R. Valerio, F. Verderame, A. Fontana, E.R. Haspinger, A. Caldara, A. Di Leone, G. Tortora, D. Giannarelli, G. Scambia, Real-world ANASTASE study of atezolizumab+nab-paclitaxel as first-line treatment of PD-L1-positive metastatic triple-negative breast cancer, npj Breast Cancer 9 (2023) 73.
[7] T. Ahmed, F.-C.F. Liu, B. Lu, H. Lip, E. Park, I. Alradwan, J.F. Liu, C. He, A. Zetrini, T. Zhang, A. Ghavaminejad, A.M. Rauth, J.T. Henderson, X.Y. Wu, Advances in nanomedicine design: multidisciplinary strategies for unmet medical needs, Mol. Pharm. 19 (2022) 1722–1765.
[8] S.K. Golombek, J.-N. May, B. Theek, L. Appold, N. Drude, F. Kiessling, T. Lammers, Tumor targeting via EPR: strategies to enhance patient responses, Adv. Drug Deliv. Rev. 130 (2018) 17–38.
[9] R. Zhu, T. Lang, Q. Yin, Y. Li, Nano drug delivery systems improve metastatic breast cancer therapy, Med. Rev. 1 (2021) (2021) 244–274.
[10] R.X. Zhang, J. Li, T. Zhang, M.A. Amini, C. He, B. Lu, T. Ahmed, H. Lip, A.M. Rauth, X.Y. Wu, Importance of integrating nanotechnology with pharmacology and physiology for innovative drug delivery and therapy – an illustration with firsthand examples, Acta Pharmacol. Sin. 39 (2018) 825–844.
[11] J. Collignon, L. Lousberg, H. Schroeder, G. Jerusalem, Triple-negative breast cancer: treatment challenges and solutions, Breast Cancer 8 (2016) 93–107.
[12] T. Safra, F. Muggia, S. Jeffers, D.D. Tsao-Wei, S. Groshen, O. Lyass, R. Henderson, G. Berry, A. Gabizon, Pegylated liposomal doxorubicin (doxil): reduced clinical cardiotoxicity in patients reaching or exceeding cumulative doses of 500 mg/m2, Ann. Oncol. 11 (2000) 1029–1033.
[13] L.Y. Li, Y.D. Guan, X.S. Chen, J.M. Yang, Y. Cheng, DNA repair pathways in cancer therapy and resistance, Front. Pharmacol. 11 (2020) 629266.
[14] D.C. Koboldt, R.S. Fulton, M.D. McLellan, H. Schmidt, J. Kalicki-Veizer, J. F. McMichael, L.L. Fulton, D.J. Dooling, L. Ding, E.R. Mardis, R.K. Wilson, A. Ally, M. Balasundaram, Y.S.N. Butterfield, R. Carlsen, C. Carter, A. Chu, E. Chuah, H.-J. E. Chun, R.J.N. Coope, N. Dhalla, R. Guin, C. Hirst, M. Hirst, R.A. Holt, D. Lee, H. I. Li, M. Mayo, R.A. Moore, A.J. Mungall, E. Pleasance, A. Gordon Robertson, J. E. Schein, A. Shafiei, P. Sipahimalani, J.R. Slobodan, D. Stoll, A. Tam, N. Thiessen, R.J. Varhol, N. Wye, T. Zeng, Y. Zhao, I. Birol, S.J.M. Jones, M.A. Marra, A. D. Cherniack, G. Saksena, R.C. Onofrio, N.H. Pho, S.L. Carter, S.E. Schumacher, B. Tabak, B. Hernandez, J. Gentry, H. Nguyen, A. Crenshaw, K. Ardlie, R. Beroukhim, W. Winckler, G. Getz, S.B. Gabriel, M. Meyerson, L. Chin, P.J. Park, R. Kucherlapati, K.A. Hoadley, J. Todd Auman, C. Fan, Y.J. Turman, Y. Shi, L. Li, M.D. Topal, X. He, H.-H. Chao, A. Prat, G.O. Silva, M.D. Iglesia, W. Zhao, J. Usary, J.S. Berg, M. Adams, J. Booker, J. Wu, A. Gulabani, T. Bodenheimer, A.P. Hoyle, J. V. Simons, M.G. Soloway, L.E. Mose, S.R. Jefferys, S. Balu, J.S. Parker, D. Neil Hayes, C.M. Perou, S. Malik, S. Mahurkar, H. Shen, D.J. Weisenberger, T. Triche Jr., P.H. Lai, M.S. Bootwalla, D.T. Maglinte, B.P. Berman, D.J. Van Den Berg, S.B. Baylin, P.W. Laird, C.J. Creighton, L.A. Donehower, G. Getz, M. Noble, D. Voet, G. Saksena, N. Gehlenborg, D. DiCara, J. Zhang, H. Zhang, C.-J. Wu, S. Yingchun Liu, M.S. Lawrence, L. Zou, A. Sivachenko, P. Lin, P. Stojanov, R. Jing, J. Cho, R. Sinha, R.W. Park, M.-D. Nazaire, J. Robinson, H. Thorvaldsdottir, J. Mesirov, P.J. Park, L. Chin, S. Reynolds, R.B. Kreisberg, B. Bernard, R. Bressler, T. Erkkila, J. Lin, V. Thorsson, W. Zhang, I. Shmulevich, G. Ciriello, N. Weinhold, N. Schultz, J. Gao, E. Cerami, B. Gross, A. Jacobsen, R. Sinha, B. Arman Aksoy, Y. Antipin, B. Reva, R. Shen, B.S. Taylor, M. Ladanyi, C. Sander, P. Anur, P. T. Spellman, Y. Lu, W. Liu, R.R.G. Verhaak, G.B. Mills, R. Akbani, N. Zhang, B. M. Broom, T.D. Casasent, C. Wakefield, A.K. Unruh, K. Baggerly, K. Coombes, J. N. Weinstein, D. Haussler, C.C. Benz, J.M. Stuart, S.C. Benz, J. Zhu, C.C. Szeto, G. K. Scott, C. Yau, E.O. Paull, D. Carlin, C. Wong, A. Sokolov, J. Thusberg, S. Mooney, S. Ng, T.C. Goldstein, K. Ellrott, M. Grifford, C. Wilks, S. Ma, B. Craft, C. Yan, Y. Hu, D. Meerzaman, J.M. Gastier-Foster, J. Bowen, N.C. Ramirez, A.D. Black, R.E. Pyatt, P. White, E.J. Zmuda, J. Frick, T.M. Lichtenberg, R. Brookens, M.M. George, M. A. Gerken, H.A. Harper, K.M. Leraas, L.J. Wise, T.R. Tabler, C. McAllister, T. Barr, M. Hart-Kothari, K. Tarvin, C. Saller, G. Sandusky, C. Mitchell, M.V. Iacocca, J. Brown, B. Rabeno, C. Czerwinski, N. Petrelli, O. Dolzhansky, M. Abramov, O. Voronina, O. Potapova, J.R. Marks, W.M. Suchorska, D. Murawa, W. Kycler, M. Ibbs, K. Korski, A. Spychała, P. Murawa, J.J. Brzeziński, H. Perz, R. Łaźniak, M. Teresiak, H. Tatka, E. Leporowska, M. Bogusz-Czerniewicz, J. Malicki, A. Mackiewicz, M. Wiznerowicz, X. Van Le, B. Kohl, N. Viet Tien, R. Thorp, N. Van Bang, H. Sussman, B. Duc Phu, R. Hajek, N. Phi Hung, T. Viet The Phuong, H. Quyet Thang, K. Zaki Khan, R. Penny, D. Mallery, E. Curley, C. Shelton, P. Yena, J. N. Ingle, F.J. Couch, W.L. Lingle, T.A. King, A. Maria Gonzalez-Angulo, G.B. Mills, M.D. Dyer, S. Liu, X. Meng, M. Patangan, N. The Cancer Genome Atlas, L. Genome sequencing centres: Washington University in St, B.C.C.A. Genome characterization centres, I. Broad, Brigham, H. Women's, S. Harvard Medical, C.H. University of North Carolina, H. University of Southern California/Johns, M. Genome data analysis: Baylor College of, B. Institute for Systems, C. Memorial Sloan-Kettering Cancer, H. Oregon, U. Science, M.D.A.C.C. The University of Texas, S.C.B.I. University of California, Nci, R. Biospecimen core resource: Nationwide Children's Hospital Biospecimen Core, A.-I. Tissue source sites, Christiana, Cureline, C. Duke University Medical, C. The Greater Poland Cancer, Ilsbio, C. International Genomics, C. Mayo, Mskcc, M.D.A.C. Center, Comprehensive molecular portraits of human breast tumours, Nature 490 (2012) 61–70.
[15] K.N. Stevens, C.M. Vachon, F.J. Couch, Genetic susceptibility to triple-negative breast cancer, Cancer Res. 73 (2013) 2025–2030.
[16] E. Franzese, S. Centonze, A. Diana, F. Carlino, L.P. Guerrera, M. Di Napoli, F. De Vita, S. Pignata, F. Ciardiello, M. Orditura, PARP inhibitors in ovarian cancer, Cancer Treat. Rev. 73 (2019) 1–9.
[17] A.M. Mendes-Pereira, S.A. Martin, R. Brough, A. McCarthy, J.R. Taylor, J.-S. Kim, T. Waldman, C.J. Lord, A. Ashworth, Synthetic lethal targeting of PTEN mutant cells with PARP inhibitors, EMBO Mol. Med. 1 (2009) 315–322.
[18] P.A. Konstantinopoulos, R. Ceccaldi, G.I. Shapiro, A.D. D'Andrea, Homologous recombination deficiency: exploiting the fundamental vulnerability of ovarian cancer, Cancer Discov. 5 (2015) 1137–1154.
[19] H. Li, Z.Y. Liu, N. Wu, Y.C. Chen, Q. Cheng, J. Wang, PARP inhibitor resistance: the underlying mechanisms and clinical implications, Mol. Cancer 19 (2020) 107.
[20] N. Johnson, S.F. Johnson, W. Yao, Y.-C. Li, Y.-E. Choi, A.J. Bernhardy, Y. Wang, M. Capelletti, K.A. Sarosiek, L.A. Moreau, Stabilization of mutant BRCA1 protein confers PARP inhibitor and platinum resistance, Proc. Natl. Acad. Sci. 110 (2013) 17041–17046.
[21] S.M. Noordermeer, H. van Attikum, PARP inhibitor resistance: a tug-of-war in BRCA-mutated cells, Trends Cell Biol. 29 (2019) 820–834.
[22] A.D. D'Andrea, Mechanisms of PARP inhibitor sensitivity and resistance, DNA Repair 71 (2018) 172–176.
[23] S. Jiao, W. Xia, H. Yamaguchi, Y. Wei, M.K. Chen, J.M. Hsu, J.L. Hsu, W.H. Yu, Y. Du, H.H. Lee, C.W. Li, C.K. Chou, S.O. Lim, S.S. Chang, J. Litton, B. Arun, G. N. Hortobagyi, M.C. Hung, PARP inhibitor upregulates PD-L1 expression and

enhances cancer-associated immunosuppression, Clin. Cancer Res. 23 (2017) 3711–3720.
[24] M.P. Dias, S.C. Moser, S. Ganesan, J. Jonkers, Understanding and overcoming resistance to PARP inhibitors in cancer therapy, Nat. Rev. Clin. Oncol. 18 (2021) 773–791.
[25] F. Peyraud, A. Italiano, Combined PARP inhibition and immune checkpoint therapy in solid tumors, Cancers (Basel) 12 (2020).
[26] L. Zhong, Y. Li, L. Xiong, W. Wang, M. Wu, T. Yuan, W. Yang, C. Tian, Z. Miao, T. Wang, S. Yang, Small molecules in targeted cancer therapy: advances, challenges, and future perspectives, Signal Transduct. Target. Ther. 6 (2021) 201.
[27] L. Carrassa, I. Colombo, G. Damia, F. Bertoni, Targeting the DNA damage response for patients with lymphoma: preclinical and clinical evidences, Cancer Treat. Rev. 90 (2020) 102090.
[28] M.D. Miljkovic, J. Tuia, T. Olivier, A. Haslam, V. Prasad, Cancer drug price and novelty in mechanism of action, JAMA Netw. Open 6 (2023) e2347006.
[29] E. Karousou, S. Misra, S. Ghatak, K. Dobra, M. Götte, D. Vigetti, A. Passi, N. K. Karamanos, S.S. Skandalis, Roles and targeting of the HAS/hyaluronan/CD44 molecular system in cancer, Matrix Biol. 59 (2017) 3–22.
[30] B.P. Toole, M.G. Slomiany, Hyaluronan, CD44 and Emmprin: partners in cancer cell chemoresistance, Drug Resist. Updat. 11 (2008) 110–121.
[31] C. Tolg, J.B. McCarthy, A. Yazdani, E.A. Turley, Hyaluronan and RHAMM in wound repair and the "cancerization" of stromal tissues, Biomed. Res. Int. 2014 (2014) 103923.
[32] S. Misra, V.C. Hascall, R.R. Markwald, S. Ghatak, Interactions between Hyaluronan and its receptors (CD44, RHAMM) regulate the activities of inflammation and cancer, Front. Immunol. 6 (2015) (201–201).
[33] M. Cohen-Armon, PARP-1 activation in the ERK signaling pathway, Trends Pharmacol. Sci. 28 (2007) 556–560.
[34] A. Kumar, O. Fernandez-Capetillo, A.C. Carrera, Nuclear phosphoinositide 3-kinase β controls double-strand break DNA repair, Proc. Natl. Acad. Sci. 107 (2010) 7491–7496.
[35] G. Guney Eskiler, M. Ozturk, Therapeutic potential of the PI3K inhibitor LY294002 and PARP inhibitor Talazoparib combination in BRCA-deficient triple negative breast cancer cells, Cell. Signal. 91 (2022) 110229.
[36] C. Sun, Y. Fang, J. Yin, J. Chen, Z. Ju, D. Zhang, X. Chen, C.P. Vellano, K.J. Jeong, P.K. Ng, A.K.B. Eterovic, N.H. Bhola, Y. Lu, S.N. Westin, J.R. Grandis, S.Y. Lin, K. L. Scott, G. Peng, J. Brugge, G.B. Mills, Rational combination therapy with PARP and MEK inhibitors capitalizes on therapeutic liabilities in RAS mutant cancers, Sci. Transl. Med. 9 (2017).
[37] Y. Gao, J.J. Yang, Y.X. Cai, S.L. Fu, N. Zhang, X.N. Fu, L.Q. Li, IFN-γ mediated inhibition of lung cancer correlates with PD-L1 expression and is regulated by PI3K-AKT signaling, Int. J. Cancer 143 (2018) 931–943.
[38] T.S. Stutvoet, A. Kol, E.G. de Vries, M. de Bruyn, R.S. Fehrmann, A.G. Terwisscha van Scheltinga, S. de Jong, MAPK pathway activity plays a key role in PD-L1 expression of lung adenocarcinoma cells, J. Pathol. 249 (2019) 52–64.
[39] S. Misra, V.C. Hascall, R.R. Markwald, S. Ghatak, Interactions between Hyaluronan and its receptors (CD44, RHAMM) regulate the activities of inflammation and cancer, Front. Immunol. 6 (2015) 201.
[40] S. Arpicco, P. Milla, B. Stella, F. Dosio, Hyaluronic acid conjugates as vectors for the active targeting of drugs, genes and nanocomposites in cancer treatment, Molecules 19 (2014) 3193–3230.
[41] P. Kesharwani, R. Chadar, A. Sheikh, W.Y. Rizg, A.Y. Safhi, CD44-targeted nanocarrier for cancer therapy, Front. Pharmacol. 12 (2022) 800481.
[42] M.G. Slomiany, L. Dai, P.A. Bomar, T.J. Knackstedt, D.A. Kranc, L. Tolliver, B. L. Maria, B.P. Toole, Abrogating drug resistance in malignant peripheral nerve sheath tumors by disrupting hyaluronan-CD44 interactions with small hyaluronan oligosaccharides, Cancer Res. 69 (2009) 4992–4998.
[43] A. Laura, B. Guillermo, A. Elida, Hyaluronan oligosaccharides sensitize lymphoma resistant cell lines to vincristine by modulating P-glycoprotein activity and PI3K/Akt pathway, Int. J. Cancer 122 (2008) 1012–1018.
[44] M. Ma, M. Weng, M. Zhang, Y. Qin, W. Gong, Z. Quan, Targeting gallbladder cancer: hyaluronan sensitizes cancer cells to chemo-therapeutics, Int. J. Clin. Exp. Pathol. 8 (2015) 1822.
[45] C. Yang, Y. Liu, Y. He, Y. Du, W. Wang, X. Shi, F. Gao, The use of HA oligosaccharide-loaded nanoparticles to breach the endogenous hyaluronan glycocalyx for breast cancer therapy, Biomaterials 34 (2013) 6829–6838.
[46] N.M. Naba, N. Tolay, B. Erman, A. Sayi Yazgan, Doxorubicin inhibits miR-140 expression and upregulates PD-L1 expression in HCT116 cells, opposite to its effects on MDA-MB-231 cells, Turk. J. Biol. 44 (2020) 15–23.
[47] D.J. Kim, J.H. Jang, S.Y. Ham, S.H. Choi, S.S. Park, S.Y. Jeong, B.C. Kim, D.Y. Jeon, B.J. Lee, B.K. Ko, J.W. Park, W.J. Cho, Doxorubicin inhibits PD-L1 expression by enhancing TTP-mediated decay of PD-L1 mRNA in cancer cells, Biochem. Biophys. Res. Commun. 522 (2020) 402–407.
[48] T. Zhang, C. Fu, I. Alradwan, T. Yen, H. Lip, P. Cai, A.M. Rauth, L. Zhang, X.Y. Wu, Targeting signaling pathways of hyaluronic acid and integrin receptors by synergistic combination nanocomposites inhibits systemic metastases and primary triple negative breast cancer, Adv. Therapeut. 4 (2021) 2100022.
[49] D. Shan, J. Li, P. Cai, P. Prasad, F. Liu, A.M. Rauth, X.Y. Wu, RGD-conjugated solid lipid nanoparticles inhibit adhesion and invasion of αvβ3 integrin-overexpressing breast cancer cells, Drug Deliv. Transl. Res. 5 (2015) 15–26.
[50] K.N. Sugahara, T. Teesalu, P.P. Karmali, V.R. Kotamraju, L. Agemy, O.M. Girard, D. Hanahan, R.F. Mattrey, E. Ruoslahti, Tissue-penetrating delivery of compounds and nanoparticles into tumors, Cancer Cell 16 (2009) 510–520.
[51] T. Zhang, H. Lip, C. He, P. Cai, Z. Wang, J.T. Henderson, A.M. Rauth, X.Y. Wu, Multitargeted nanoparticles deliver synergistic drugs across the blood–brain barrier to brain metastases of triple negative breast cancer cells and tumor-associated macrophages, Adv. Healthc. Mater. 8 (2019) 1900543.
[52] R. Dissanayake, R. Towner, M. Ahmed, Metastatic breast Cancer: review of emerging Nanotherapeutics, Cancers (Basel) 15 (2023).
[53] J. Li, P. Cai, A. Shalviri, J.T. Henderson, C. He, W.D. Foltz, P. Prasad, P. M. Brodersen, Y. Chen, R. DaCosta, A.M. Rauth, X.Y. Wu, A multifunctional polymeric nanotheranostic system delivers doxorubicin and imaging agents across the blood-brain barrier targeting brain metastases of breast cancer, ACS Nano 8 (2014) 9925–9940.
[54] A.J. Shuhendler, P. Prasad, M. Leung, A.M. Rauth, R.S. Dacosta, X.Y. Wu, A novel solid lipid nanoparticle formulation for active targeting to tumor alpha(v) beta(3) integrin receptors reveals cyclic RGD as a double-edged sword, Adv. Healthc. Mater. 1 (2012) 600–608.
[55] D. Shan, J. Li, P. Cai, P. Prasad, F. Liu, A.M. Rauth, X.Y. Wu, RGD-conjugated solid lipid nanoparticles inhibit adhesion and invasion of alphavbeta3 integrin-overexpressing breast cancer cells, Drug Deliv. Transl. Res. 5 (2015) 15–26.
[56] M.J. Abdekhodaie, Z. Liu, S.Z. Erhan, X.Y. Wu, Characterization of novel soybean-oil-based thermosensitive amphiphilic polymers for drug delivery applications, Polym. Int. 61 (2012) 1477–1484.
[57] T. Zhang, P. Prasad, P. Cai, C. He, D. Shan, A.M. Rauth, X.Y. Wu, Dual-targeted hybrid nanoparticles of synergistic drugs for treating lung metastases of triple negative breast cancer in mice, Acta Pharmacol. Sin. 38 (2017) 835–847.
[58] A.J. Shuhendler, P. Prasad, R.X. Zhang, M.A. Amini, M. Sun, P.P. Liu, R.G. Bristow, A.M. Rauth, X.Y. Wu, Synergistic nanoparticulate drug combination overcomes multidrug resistance, increases efficacy, and reduces cardiotoxicity in a nonimmunocompromised breast tumor model, Mol. Pharm. 11 (2014) 2659–2674.
[59] Y. Qu, B. Han, Y. Yu, W. Yao, S. Bose, B.Y. Karlan, A.E. Giuliano, X. Cui, Evaluation of MCF10A as a reliable model for Normal human mammary epithelial cells, PLoS One 10 (2015) e0131285.
[60] C. Singh, R.K. Shyanti, V. Singh, R.K. Kale, J.P.N. Mishra, R.P. Singh, Integrin expression and glycosylation patterns regulate cell-matrix adhesion and alter with breast cancer progression, Biochem. Biophys. Res. Commun. 499 (2018) 374–380.
[61] S.R. Hamilton, S.F. Fard, F.F. Paiwand, C. Tolg, M. Veiseh, C. Wang, J.B. McCarthy, M.J. Bissell, J. Koropatnick, E.A. Turley, The hyaluronan receptors CD44 and Rhamm (CD168) form complexes with ERK1,2 that sustain high basal motility in breast cancer cells, J. Biol. Chem. 282 (2007) 16667–16680.
[62] S. Jiao, W. Xia, H. Yamaguchi, Y. Wei, M.-K. Chen, J.-M. Hsu, J.L. Hsu, W.-H. Yu, Y. Du, H.-H. Lee, C.-W. Li, C.-K. Chou, S.-O. Lim, S.-S. Chang, J. Litton, B. Arun, G. N. Hortobagyi, M.-C. Hung, PARP inhibitor upregulates PD-L1 expression and enhances Cancer-associated immunosuppression, Clin. Cancer Res. 23 (2017) 3711–3720.
[63] K.N. Dziadkowiec, E. Gąsiorowska, E. Nowak-Markwitz, A. Jankowska, PARP inhibitors: review of mechanisms of action and BRCA1/2 mutation targeting, Przeglad Menopauzalny 15 (2016) 215–219.
[64] A.K. Mehta, E.M. Cheney, C.A. Hartl, C. Pantelidou, M. Oliwa, J.A. Castrillon, J.-R. Lin, K.E. Hurst, M. de Oliveira Taveira, N.T. Johnson, W.M. Oldham, M. Kalocsay, M.J. Berberich, S.A. Boswell, A. Kothari, S. Johnson, D.A. Dillon, M. Lipschitz, S. Rodig, S. Santagata, J.E. Garber, N. Tung, J. Yélamos, J.E. Thaxton, E.A. Mittendorf, P.K. Sorger, G.I. Shapiro, J.L. Guerriero, Targeting immunosuppressive macrophages overcomes PARP inhibitor resistance in BRCA1-associated triple-negative breast cancer, Nat. Can. 2 (2021) 66–82.
[65] C.-P. Chou, S.S. Jiang, H.-B. Pan, Y.-C. Yen, H.-H. Tseng, Y.-T. Hung, S.-H. Wang, Y.-L. Chen, Y.-W. Chen, Endothelial cell colony forming units derived from malignant breast diseases are resistant to tumor necrosis factor-α-induced apoptosis, Sci. Rep. 6 (2016) 37450.
[66] E. Abad, L. Civit, D. Potesil, Z. Zdrahal, A. Lyakhovich, Enhanced DNA damage response through RAD50 in triple negative breast cancer resistant and cancer stem-like cells contributes to chemoresistance, FEBS J. 288 (7) (2020) 2184–2202.
[67] C.G. Broustas, H.B. Lieberman, DNA damage response genes and the development of cancer metastasis, Radiat. Res. 181 (2014) 111–130.
[68] A. Ivashkevich, C.E. Redon, A.J. Nakamura, R.F. Martin, O.A. Martin, Use of the γ-H2AX assay to monitor DNA damage and repair in translational cancer research, Cancer Lett. 327 (2012) 123–133.
[69] D. Plesca, S. Mazumder, A. Almasan, DNA damage response and apoptosis, Methods Enzymol. 446 (2008) 107–122.
[70] M. Cohen-Armon, L. Visochek, D. Rozensal, A. Kalal, I. Geistrikh, R. Klein, S. Bendetz-Nezer, Z. Yao, R. Seger, DNA-independent PARP-1 activation by phosphorylated ERK2 increases Elk1 activity: a link to histone acetylation, Mol. Cell 25 (2007) 297–308.
[71] T.M. Kauppinen, W.Y. Chan, S.W. Suh, A.K. Wiggins, E.J. Huang, R.A. Swanson, Direct phosphorylation and regulation of poly(ADP-ribose) polymerase-1 by extracellular signal-regulated kinases 1/2, Proc. Natl. Acad. Sci. 103 (2006) 7136–7141.
[72] A. Yacoub, J.S. Park, L. Qiao, P. Dent, M.P. Hagan, MAPK dependence of DNA damage repair: ionizing radiation and the induction of expression of the DNA repair genes XRCC1 and ERCC1 in DU145 human prostate carcinoma cells in a MEK1/2 dependent fashion, Int. J. Radiat. Biol. 77 (2001) 1067–1078.
[73] M. Cohen-Armon, PARP-1 activation in the ERK signaling pathway, Trends Pharmacol. Sci. 28 (2007) 556–560.
[74] H. Wei, X. Yu, Functions of PARylation in DNA damage repair pathways, Genomics Proteomics Bioinformatics 14 (2016) 131–139.
[75] K.J. Lastwika, W. Wilson 3rd, Q.K. Li, J. Norris, H. Xu, S.R. Ghazarian, H. Kitagawa, S. Kawabata, J.M. Taube, S. Yao, L.N. Liu, J.J. Gills, P.A. Dennis, Control of PD-L1 expression by oncogenic activation of the AKT-mTOR pathway in non-small cell lung cancer, Cancer Res. 76 (2016) 227–238.

[76] C.A. Crane, A. Panner, J.C. Murray, S.P. Wilson, H. Xu, L. Chen, J.P. Simko, F. M. Waldman, R.O. Pieper, A.T. Parsa, PI(3) kinase is associated with a mechanism of immunoresistance in breast and prostate cancer, Oncogene 28 (2009) 306–312.
[77] A.T. Parsa, J.S. Waldron, A. Panner, C.A. Crane, I.F. Parney, J.J. Barry, K. E. Cachola, J.C. Murray, T. Tihan, M.C. Jensen, P.S. Mischel, D. Stokoe, R. O. Pieper, Loss of tumor suppressor PTEN function increases B7-H1 expression and immunoresistance in glioma, Nat. Med. 13 (2007) 84–88.
[78] F. Mateo, Z. He, L. Mei, G.R. de Garibay, C. Herranz, N. García, A. Lorentzian, A. Baiges, E. Blommaert, A. Gómez, O. Mirallas, A. Garrido-Utrilla, L. Palomero, R. Espín, A.I. Extremera, M.T. Soler-Monsó, A. Petit, R. Li, J. Brunet, K. Chen, S. Tan, C.J. Eaves, C. McCloskey, R. Hakem, R. Khokha, P.F. Lange, C. Lázaro, C. A. Maxwell, M.A. Pujana, Modification of BRCA1-associated breast cancer risk by HMMR overexpression, Nat. Commun. 13 (2022) 1895.
[79] C.A. Maxwell, J. Benítez, L. Gómez-Baldó, A. Osorio, N. Bonifaci, R. Fernández-Ramires, S.V. Costes, E. Guinó, H. Chen, G.J. Evans, P. Mohan, I. Català, A. Petit, H. Aguilar, A. Villanueva, A. Aytes, J. Serra-Musach, G. Rennert, F. Lejbkowicz, P. Peterlongo, S. Manoukian, B. Peissel, C.B. Ripamonti, B. Bonanni, A. Viel, A. Allavena, L. Bernard, P. Radice, E. Friedman, B. Kaufman, Y. Laitman, M. Dubrovsky, R. Milgrom, A. Jakubowska, C. Cybulski, B. Gorski, K. Jaworska, K. Durda, G. Sukiennicki, J. Lubiński, Y.Y. Shugart, S.M. Domchek, R. Letrero, B. L. Weber, F.B. Hogervorst, M.A. Rookus, J.M. Collee, P. Devilee, M.J. Ligtenberg, R.B. Luijt, C.M. Aalfs, Q. Waisfisz, J. Wijnen, C.E. Roozendaal, D.F. Easton, S. Peock, M. Cook, C. Oliver, D. Frost, P. Harrington, D.G. Evans, F. Lalloo, R. Eeles, L. Izatt, C. Chu, D. Eccles, F. Douglas, C. Brewer, H. Nevanlinna, T. Heikkinen, F. J. Couch, N.M. Lindor, X. Wang, A.K. Godwin, M.A. Caligo, G. Lombardi, N. Loman, P. Karlsson, H. Ehrencrona, A. Wachenfeldt, R.B. Barkardottir, U. Hamann, M.U. Rashid, A. Lasa, T. Caldés, R. Andrés, M. Schmitt, V. Assmann, K. Stevens, K. Offit, J. Curado, H. Tilgner, R. Guigó, G. Aiza, J. Brunet, J. Castellsagué, G. Martrat, A. Urruticoechea, I. Blanco, L. Tihomirova, D. E. Goldgar, S. Buys, E.M. John, A. Miron, M. Southey, M.B. Daly, R.K. Schmutzler, B. Wappenschmidt, A. Meindl, N. Arnold, H. Deissler, R. Varon-Mateeva, C. Sutter, D. Niederacher, E. Imyamitov, O.M. Sinilnikova, D. Stoppa-Lyonne, S. Mazoyer, C. Verny-Pierre, L. Castera, A. de Pauw, Y.J. Bignon, N. Uhrhammer, J.P. Peyrat, P. Vennin, S. Fert Ferrer, M.A. Collonge-Rame, I. Mortemousque, A.B. Spurdle, J. Beesley, X. Chen, S. Healey, M.H. Barcellos-Hoff, M. Vidal, S.B. Gruber, C. Lázaro, G. Capellá, L. McGuffog, K.L. Nathanson, A.C. Antoniou, G. Chenevix-Trench, M.C. Fleisch, V. Moreno, M.A. Pujana, Interplay between BRCA1 and RHAMM regulates epithelial apicobasal polarization and may influence risk of breast cancer, PLoS Biol. 9 (2011) (e1001199).
[80] J. Chang, G.M. Clark, D.C. Allred, S. Mohsin, G. Chamness, R.M. Elledge, Survival of patients with metastatic breast carcinoma: importance of prognostic markers of the primary tumor, Cancer 97 (2003) 545–553.
[81] C. Liedtke, C. Mazouni, K.R. Hess, F. Andre, A. Tordai, J.A. Mejia, W.F. Symmans, A.M. Gonzalez-Angulo, B. Hennessy, M. Green, M. Cristofanilli, G.N. Hortobagyi, L. Pusztai, Response to neoadjuvant therapy and long-term survival in patients with triple-negative breast cancer, J. Clin. Oncol. 41 (2023) 1809–1815.